Mineralogical Magazine (2020), **84**, 839–853
doi:10.1180/mgm.2020.64

CAMBRIDGE UNIVERSITY PRESS

Article

The mineralogy of the historical Mochalin Log *REE* deposit, South Urals, Russia. Part II. Radekškodaite-(La), $(CaLa_5)(Al_4Fe^{2+})[Si_2O_7][SiO_4]_5O(OH)_3$ and radekškodaite-(Ce), $(CaCe_5)(Al_4Fe^{2+})[Si_2O_7][SiO_4]_5O(OH)_3$, two new minerals with a novel structure-type belonging to the epidote–törnebohmite polysomatic series

Anatoly V. Kasatkin[1]*, Natalia V. Zubkova[2], Igor V. Pekov[2,3], Nikita V. Chukanov[4], Dmitriy A. Ksenofontov[2], Atali A. Agakhanov[1], Dmitriy I. Belakovskiy[1], Yury S. Polekhovsky[5,†], Aleksey M. Kuznetsov[6], Sergey N. Britvin[5], Dmitry Yu. Pushcharovsky[2] and Fabrizio Nestola[7]

[1]Fersman Mineralogical Museum of the Russian Academy of Sciences, Leninsky Prospekt 18-2, 119071 Moscow, Russia; [2]Faculty of Geology, Moscow State University, Vorobievy Gory, 119991 Moscow, Russia; [3]Vernadsky Institute of Geochemistry and Analytical Chemistry, Russian Academy of Sciences, Kosygina str. 19, 119991 Moscow, Russia; [4]Institute of Problems of Chemical Physics, Russian Academy of Sciences, 142432 Chernogolovka, Moscow region, Russia; [5]Institute of Earth Sciences, St Petersburg State University, University Embankment 7/9, 199034 St Petersburg, Russia; [6]Oktyabrskaya str., 5-337, 454071 Chelyabinsk, Russia; and [7]Dipartimento di Geoscienze, Università di Padova, Via Gradenigo 6, I-35131, Padova, Italy.

Abstract

Two new isostructural minerals radekškodaite-(La) $(CaLa_5)(Al_4Fe^{2+})[Si_2O_7][SiO_4]_5O(OH)_3$ and radekškodaite-(Ce) $(CaCe_5)(Al_4Fe^{2+})[Si_2O_7][SiO_4]_5O(OH)_3$ were discovered in polymineralic nodules from the Mochalin Log *REE* deposit, South Urals, Russia. Radekškodaite-(La) is associated with allanite-(Ce), allanite-(La), bastnäsite-(Ce), bastnäsite-(La), ferriallanite-(Ce), ferriallanite-(La), ferriperbøeite-(La), fluorbritholite-(Ce), törnebohmite-(Ce) and törnebohmite-(La). Radekškodaite-(Ce) is associated with ancylite-(Ce), bastnäsite-(Ce), bastnäsite-(La), lanthanite-(La), perbøeite-(Ce) and törnebohmite-(Ce). The new minerals form isolated anhedral grains up to 0.35 × 0.75 mm [radekškodaite-(La)] and 1 mm × 2 mm [radekškodaite-(Ce)]. Both minerals are greenish-brown with vitreous lustre. $D_{calc} = 4.644$ [radekškodaite-(La)] and 4.651 [radekškodaite-(Ce)] g cm^{-3}. Both minerals are optically biaxial (+); radekškodaite-(La): $\alpha = 1.790(7)$, $\beta = 1.798(5)$, $\gamma = 1.825(8)$ and $2V_{meas} = 60(10)°$; radekškodaite-(Ce): $\alpha = 1.798(6)$, $\beta = 1.806(6)$, $\gamma = 1.833(8)$ and $2V_{meas} = 65(10)°$. Chemical data [wt.%, electron-microprobe; FeO:Fe_2O_3 by charge balance; H_2O by stochiometry; radekškodaite-(La)/radekškodaite-(Ce)] are: CaO 3.40/2.74, La_2O_3 27.68/22.23, Ce_2O_3 20.39/24.30, Pr_2O_3 0.94/1.48, Nd_2O_3 1.71/3.18, ThO_2 0.23/0.24, MgO 0.85/1.04, Al_2O_3 10.35/10.84, MnO 0.64/0.69, FeO 2.55/2.76, Fe_2O_3 3.12/2.57, TiO_2 0.13/0.04, SiO_2 26.03/26.10, F 0.10/0.09, H_2O 1.62/1.63, –O=F –0.04/–0.04, total 99.70/99.89. The empirical formulae based on $O_{28}(OH,F)_3$ are: radekškodaite-(La): $(Ca_{0.98}Th_{0.01}La_{2.75}Ce_{2.01}Nd_{0.16}Pr_{0.09})_{\Sigma 6.00}(Al_{3.28}Fe^{3+}_{0.63}Fe^{2+}_{0.57}Mg_{0.34}Mn_{0.15}Ti_{0.03})_{\Sigma 5.00}Si_{7.00}O_{28}[(OH)_{2.91}F_{0.09}]$; radekškodaite-(Ce): $(Ca_{0.79}Mn_{0.16}Th_{0.01}Ce_{2.39}La_{2.20}Nd_{0.30}Pr_{0.14})_{\Sigma 5.99}(Al_{3.43}Fe^{2+}_{0.62}Fe^{3+}_{0.52}Mg_{0.42}Ti_{0.01})_{\Sigma 5.00}Si_{7.00}O_{28}[(OH)_{2.92}F_{0.08}]$. Both minerals are monoclinic, $P2_1/m$; the unit-cell parameters [radekškodaite-(La)/radekškodaite-(Ce)] are: $a = 8.9604(3)/8.9702(4)$, $b = 5.7268(2)/5.7044(2)$, $c = 25.1128(10)/25.1642(13)$ Å, $\beta = 116.627(5)/116.766(6)°$, $V = 1151.98(7)/1149.68(11)$ Å^3 and $Z = 2/2$. The crystal structures are solved based on single-crystal X-ray diffraction data; $R = 0.0554$ [radekškodaite-(La)] and 0.0769 [radekškodaite-(Ce)]. Both minerals belong to the epidote–törnebohmite polysomatic series and represent first members of **ET2**-type: their structure consists of regular alternating modules, one slab of the epidote (E) structure and two slabs of törnebohmite (T). The root-name radekškodaite is given in honor of the Czech mineralogist Radek Škoda (born 1979), Associate Professor at Masaryk University, Brno, Czech Republic. The suffix-modifier -(La) or -(Ce) indicates the predominance of La or Ce among *REE* in the mineral.

Keywords: radekškodaite-(La), radekškodaite-(Ce), new mineral, rare-earth silicate, crystal structure, polysomatism, allanite, törnebohmite, Mochalin Log, South Urals

(Received 17 June 2020; accepted 9 August 2020; Accepted Manuscript published online: 24 August 2020; Associate Editor: Irina O Galuskina)

*Author for correspondence: Anatoly V. Kasatkin, E-mail: anatoly.kasatkin@gmail.com
†Deceased 28 September 2018.

Cite this article: Kasatkin A.V., Zubkova N.V., Pekov I.V., Chukanov N.V., Ksenofontov D.A., Agakhanov A.A., Belakovskiy D.I., Polekhovsky Y.S., Kuznetsov A.M., Britvin S.N., Pushcharovsky D.Y.u. and Nestola F. (2020) The mineralogy of the historical Mochalin Log *REE* deposit, South Urals, Russia. Part II. Radekškodaite-(La), $(CaLa_5)(Al_4Fe^{2+})[Si_2O_7][SiO_4]_5O(OH)_3$ and radekškodaite-(Ce), $(CaCe_5)(Al_4Fe^{2+})[Si_2O_7][SiO_4]_5O(OH)_3$, two new minerals with a novel structure-type belonging to the epidote–törnebohmite polysomatic series. *Mineralogical Magazine* **84**, 839–853. https://doi.org/10.1180/mgm.2020.64

Introduction

This article is the second in a series of papers on the mineralogical description and crystal chemistry of minerals containing rare earth elements (*REE*) as species-defining cations (henceforth – '*REE* minerals') from polymineralic nodules found at the Mochalin Log deposit, Chelyabinsk Oblast, South Urals, Russia

(55°48′42″N, 60°33′46″E). A brief outline of the history of studies, the general data on geology and mineralogy of this deposit, as well as the description of two new isostructural gatelite-group minerals, ferriperbøeite-(La) and perbøeite-(La) are given in the first paper of this series (Kasatkin *et al.*, 2020b) and references therein.

In the present article we describe two new isostructural minerals, radekškodaite-(La) [pronounced: ra dek shko da ait; Russian Cyrillic: радекшкодаит-(La)], ideally $(CaLa_5)(Al_4Fe^{2+})[Si_2O_7][SiO_4]_5O(OH)_3$, and radekškodaite-(Ce) [Russian Cyrillic: радекшкодаит-(Ce)], ideally $(CaCe_5)(Al_4Fe^{2+})[Si_2O_7][SiO_4]_5O(OH)_3$. Radekškodaite-(La), the member of this pair discovered first, was named in honour of Dr. Radek Škoda (born 1979), Associate Professor at the Department of Geological Sciences, Faculty of Science, Masaryk University, Brno, Czech Republic. Dr. Škoda is known for his contribution to the mineralogy and geochemistry of *REE* – see, e.g. Škoda and Novák (2007), Škoda *et al.* (2011, 2012, 2015, 2018), Breiter *et al.* (2009), Čopjakova *et al.* (2013, 2015), Hönig *et al.* (2014), Plášil and Škoda (2017) and Plášil *et al.* (2018). In addition, once the new phase was discovered during routine scanning electron microscope (SEM) energy-dispersive spectroscopy studies, Dr Škoda made an assumption that it might be the first member of a well-known '**ET**' (epidote–törnebohmite) polysomatic series including one epidote and two törnebohmite modules (that we propose below to name **ET2**) in contrast with all the other members of the series based on 1:1 alternation (**ET**). Subsequent structural investigations have now superbly confirmed his hypothesis. The Levinson suffix-modifier -(La) in the mineral name reflects the predominance of La among *REE*. Radekškodaite-(Ce) was named as an analogue of radekškodaite-(La) with Ce predominant over each of the other *REE*.

Both new minerals and their names have been approved by the Commission on New Minerals, Nomenclature and Classification of the International Mineralogical Association (IMA): IMA2018-107 [radekškodaite-(La), Kasatkin *et al.*, 2018] and IMA2019-042 [radekškodaite-(Ce), Kasatkin *et al.*, 2019b]. The type specimens are deposited in the systematic collection of the Fersman Mineralogical Museum of the Russian Academy of Sciences, Moscow with the catalogue numbers 96279 [radekškodaite-(La)] and 96698 [radekškodaite-(Ce)].

Occurrence and general appearance

Polymineralic nodules containing both new minerals were found in the 1980s by local collectors at the historical dump no. 2 (Fig. 1) within the Mochalin Log valley and then deposited in the collection of one of the authors (A.M.K.). In 2017 they were sent to the senior author for routine electron microprobe analysis (EMPA) that revealed the novelty of two *REE*-bearing phases and started the complex investigation into them as new mineral species.

As has been mentioned by Kasatkin *et al.* (2020b), one of the most characteristic features of *REE* minerals from Mochalin Log is that in the majority of samples the gross Ce:La ratio varies widely but is most frequently close to 1:1 so that both Ce- and La-dominant members may occur in the same specimen. Therefore, in the text below, the absence of a particular Levinson suffix means the presence of Ce- and La-dominant mineral species together.

Radekškodaite-(La) occurs in polymineralic nodules composed mainly of allanite–ferriallanite, bastnäsite, fluorbritholite-(Ce) and törnebohmite. The new mineral is typically intergrown with ferriperbøeite-(La) (Kasatkin *et al.*, 2020b) or is overgrown by it and often contains small inclusions of allanite–ferriallanite (Fig. 2). Other minerals associated closely with radekškodaite-(La) include albite, alexkuznetsovite-(Ce) (Kasatkin *et al.*, 2020a), alexkuznetsovite-(La) (Kasatkin *et al.*, 2019a), biraite-(Ce), cerianite-(Ce), *REE*-bearing epidote, ferriperbøeite-(Ce), heulandite-Ca, hollandite, lanthanite-(La), monazite, nontronite, perbøeite, perrierite, rhabdophane-(La), thorianite and thorite.

Fig. 1. Radek Škoda (left) and Anatoly V. Kasatkin (right) at historical dump No. 2 where nodules containing radekškodaite-(La) and radekškodaite-(Ce) were collected. The memorial plate between them says that Mochalin Log was visited in 1912 by Academician A.E. Fersman. August 2018. Photo: A.M. Kuznetsov.

Radekškodaite-(Ce) occurs in polymineralic nodules composed mainly of bastnäsite, perbøeite-(Ce) and törnebohmite-(Ce) (Fig. 3). Other minerals present in the association with radekškodaite-(Ce) are allanite-(Ce), ancylite-(Ce), cerianite-(Ce), ferriallanite-(Ce), heulandite-Ca, lanthanite-(La), magnetite, perrierite-(Ce), quartz, thorianite and thorite.

According to the distribution scale of *REE* minerals found at the Mochalin Log deposit (Kasatkin *et al.*, 2020b), radekškodaite-(La) should be considered as rare and radekškodaite-(Ce) as very rare: among 300 nodules with *REE*-bearing minerals investigated by us, radekškodaite-(La) was found in 13 and radekškodaite-(Ce) only in two. These new minerals were not found in association with each other.

Both new minerals form isolated anhedral grains. Those of radekškodaite-(La) reach 0.35 mm × 0.75 mm, but typically they are much smaller. Although radekškodaite-(Ce) is rarer, its grains are bigger (up to 1 mm × 2 mm in the holotype specimen).

Physical properties and optical data

Both new minerals are greenish-brown, translucent in thin fragments, with brown streak and vitreous lustre. They are non-fluorescent under ultraviolet light. One direction of good cleavage and one direction of imperfect cleavage are observed. Based on the structure data (see below) we assume that good cleavage could be on {100}. Both minerals are brittle with an uneven fracture (observed under the SEM). The Vickers' hardness (load 150 g) is equal to 871 kg mm^{-2} (range 804–919, $n = 5$) for radekškodaite-(La) and to 862 kg mm^{-2} (range 800–922, $n = 5$) for radekškodaite-(Ce); both values correspond to *ca.* 6½ on the Mohs scale. Density could not be measured due to lack of pure material in grains suitable for measurements. Density values calculated using the empirical formulae and the unit-cell parameters

https://doi.org/10.1180/mgm.2020.64 Published online by Cambridge University Press

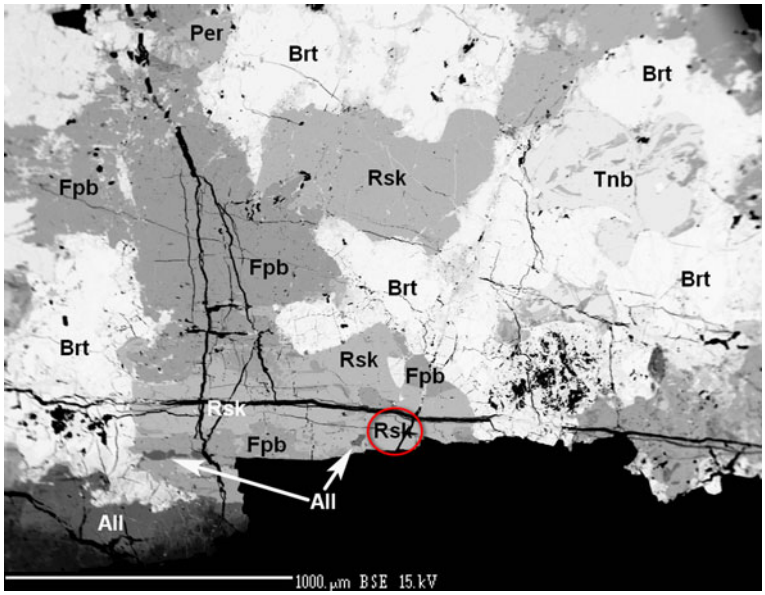

Fig. 2. Radekškodaite-(La) (Rsk) associated with ferriperbøeite-(La) (Fpb), fluorbritholite-(Ce) (Brt), allanite-(La) (All), törnebohmite-(La) (Tnb) and perrierite-(La) (Per). Black grains are quartz. The red circle shows the place from which the new mineral was extracted for the structural investigation. Polished section, specimen no. ML 60-2. SEM (back-scattered electron) image.

from single-crystal X-ray diffraction (XRD) data are 4.644 g cm^{-3} for radekškodaite-(La) and 4.651 g cm^{-3} for radekškodaite-(Ce).

Both new species are weakly pleochroic in marsh green hues with the absorption scheme $Z > Y > X$. Some areas found in grains of radekškodaite-(La) have a weak pleochroism in brownish tints with the same absorption scheme. Both minerals are optically biaxial (+). Radekškodaite-(La) has $\alpha = 1.790(7)$, $\beta = 1.798(5)$, $\gamma = 1.825(8)$ (589 nm), $2V = 60(10)°$ and $2V_{calc} = 58°$. Radekškodaite-(Ce) has $\alpha = 1.798(6)$, $\beta = 1.806(6)$, $\gamma = 1.833(8)$ (589 nm), $2V = 65(10)°$ and $2V_{calc} = 58°$. The 2V values are estimated by the curvature degree of the isogyre on the sections perpendicular to the optical axes. In both cases dispersion of optical axes is weak, $r < v$. Optical orientation was not determined for either mineral due to the anhedral shape of the grains.

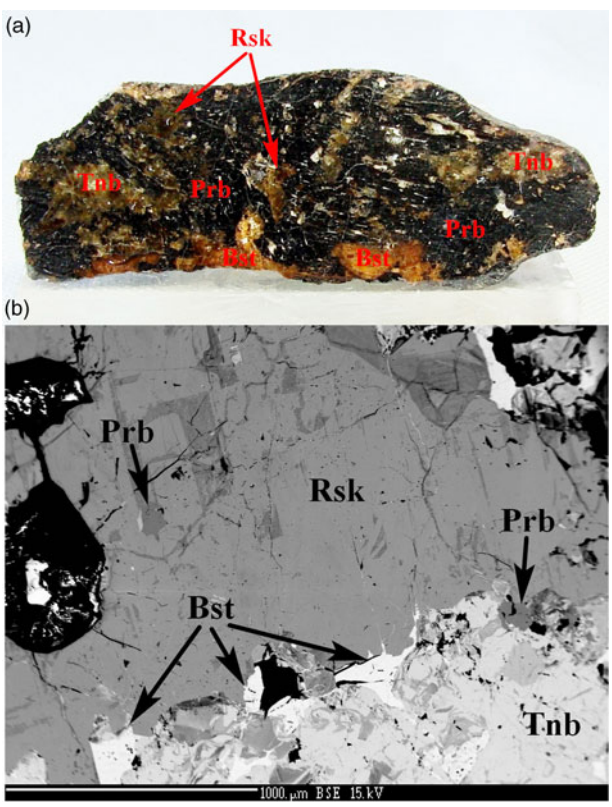

Fig. 3. (*a*) Polished section of a nodule showing zones of brown radekškodaite-(Ce) (Rsk), black perbøeite-(Ce) (Prb), orange–yellow bastnäsite-(Ce)/-(La) (Bst) and greenish törnebohmite-(Ce) (Tnb). Size of the sample: 3.9 cm × 1.4 cm; (*b*) SEM (back-scattered electron) image on a fragment from (*a*), specimen no. ML 85-2. Black grains are quartz.

Optical properties of radekškodaite-(La) were also examined in reflected light. The mineral is dark grey, very weakly anisotropic with whitish internal reflections. The bireflectance is very weak, $\Delta R = 0.2\%$ (589 nm). The reflectance values have been measured in air by means of the MSF-21 microspectrophotometer (LOMO company, St. Petersburg, Russia) with the monochromator slit width of 0.4 mm and beam diameter of 0.1 mm. SiC (Reflectionstandard 474251, No. 545, Germany) was used as a standard. The reflectance values (R_{max}/R_{min}) are given in Table 1.

The Gladstone-Dale compatibility index ($1 - K_p/K_c$) is 0.036 for radekškodaite-(La) and 0.022 for radekškodaite-(Ce) using their empirical formulae and the unit-cell parameters determined from single-crystal X-ray data. Both values are rated as excellent (Mandarino, 1981).

Radekškodaite-(La) and radekškodaite-(Ce) do not react with cold hydrochloric and nitric acids.

Table 1. Reflectance data (R, %) of radekškodaite-(La).

λ (nm)	R_{max}	R_{min}	λ (nm)	R_{max}	R_{min}
400	8.9	8.7	560	8.5	8.3
420	8.8	8.6	580	8.5	8.3
440	8.7	8.5	**589**	**8.5**	**8.3**
460	8.6	8.5	600	8.5	8.3
470	**8.6**	**8.4**	620	8.5	8.3
480	8.6	8.4	640	8.4	8.3
500	8.6	8.4	**650**	**8.4**	**8.3**
520	8.6	8.4	660	8.4	8.3
540	8.5	8.4	680	8.4	8.3
546	**8.5**	**8.4**	700	8.4	8.2

Data for wavelengths recommended by the IMA Commission on ore microscopy (COM) are marked in boldtype.

https://doi.org/10.1180/mgm.2020.64 Published online by Cambridge University Press

Raman spectroscopy

The Raman spectra (Figs 4 and 5) of radekškodaite-(La) and radekškodaite-(Ce) were obtained from polished sections by means of a Horiba Labram HR Evolution spectrometer. This dispersive, edge-filter-based system is equipped with an Olympus BX 41 optical microscope, a diffraction grating with 600 grooves per millimetre, and a Peltier-cooled, Si-based charge-coupled device (CCD) detector. After careful tests with different lasers (473, 532 and 633 nm), the 633 nm He–Ne laser with the beam power of 10 mW at the sample surface was selected for spectra acquisition to minimise analytical artefacts. A Raman signal was collected in the range of 100–4000 cm^{-1} with a 100x objective and the system operating in the confocal mode; beam diameter was ~1 μm and the lateral resolution ~2 μm. No visual damage of the analysed surface was observed at these conditions after the excitation. Wavenumber calibration was done using the Rayleigh line and low-pressure Ne-discharge lamp emissions. The wavenumber accuracy was ~0.5 cm^{-1}, and the spectral resolution was ~2 cm^{-1}. Band fitting was done after appropriate background correction, assuming combined Lorentzian–Gaussian band shapes using the Voight function (*PeakFit*; Jandel Scientific Software).

The spectra of both new minerals are similar; the small differences are mainly in the ratios of band intensities and probably are of an orientational nature. In the Raman spectra of radekškodaite-(La) and radekškodaite-(Ce), three bands of O–H stretching vibrations are observed, which corresponds to the number of independent sites occupied by OH groups. Bands at 3438, 3337 and 3225 cm^{-1} in the spectrum of radekškodaite-(La) and 3384, 3325 and 3216 cm^{-1} in the spectrum of radekškodaite-(Ce)

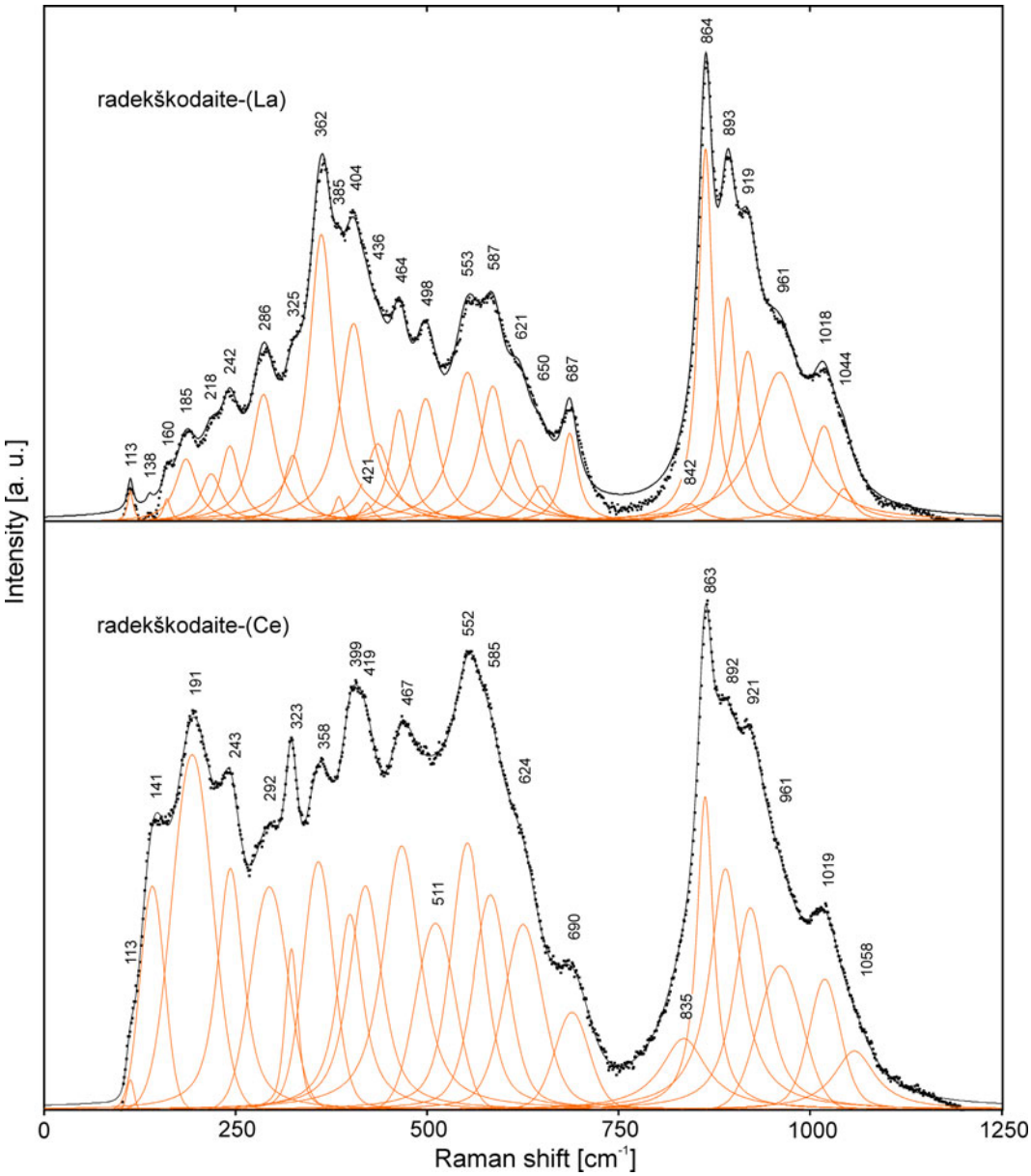

Fig. 4. Raman spectra of radekškodaite-(La) and radekškodaite-(Ce) excited by a 633 nm laser in the 100–1250 cm^{-1} region. The measured spectrum is shown by dots. The curve matched to dots is a result of spectral fit as a sum of individual Voigt peaks shown below the curve.

https://doi.org/10.1180/mgm.2020.64 Published online by Cambridge University Press

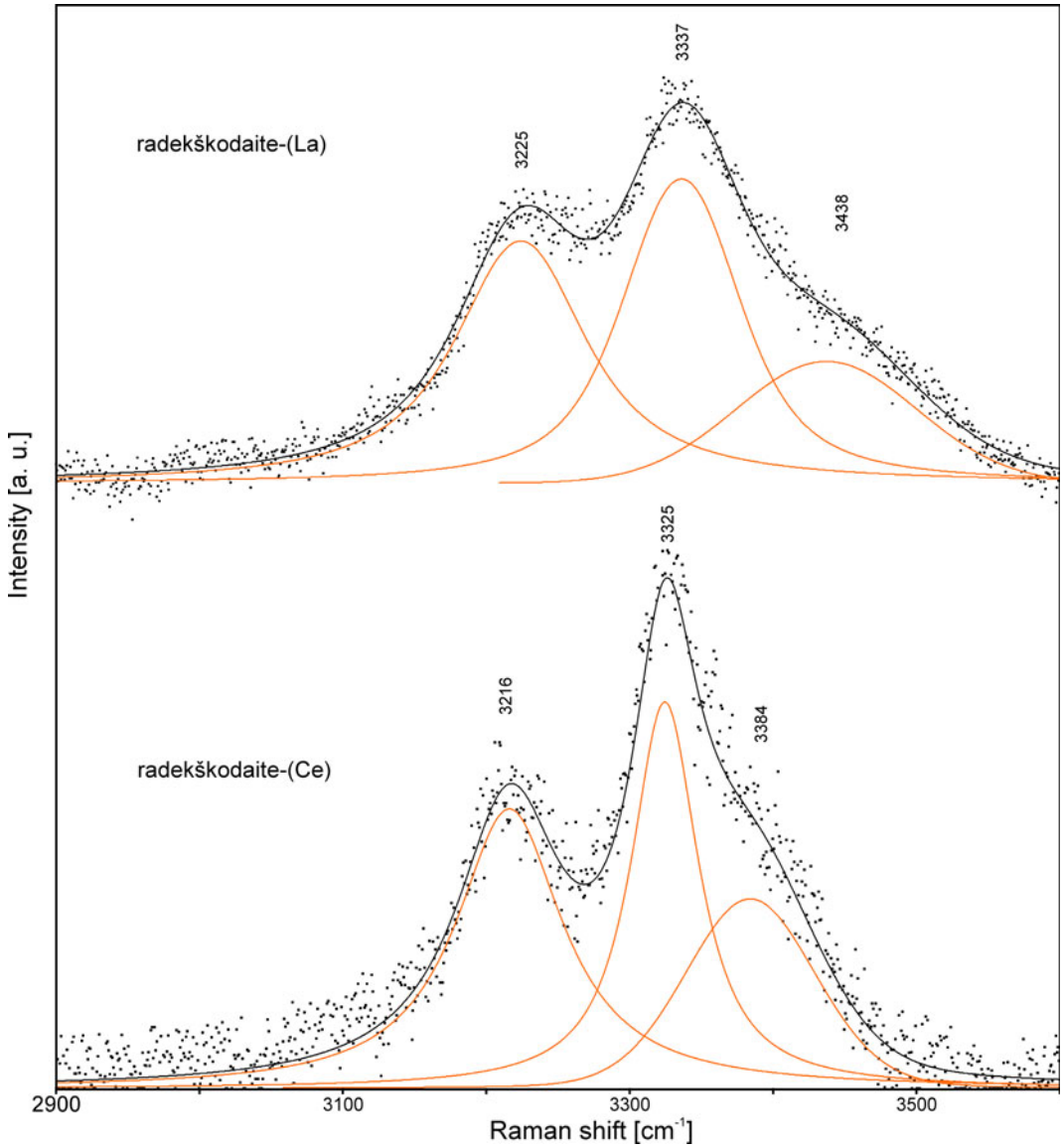

Fig. 5. Raman spectra of radekškodaite-(La) and radekškodaite-(Ce) excited by a 633 nm laser in the 2900–3600 cm^{-1} region. The measured spectrum is shown by dots. The curve matched to dots is a result of spectral fit as a sum of individual Voigt peaks shown below the curve.

correspond to O–H-stretching vibrations of the O2–H, O1–H and O3–H groups, respectively (the assignment was made based on H· · ·*A* distances equal to 2.968, 2.718 and 2.710 Å, respectively, in radekškodaite-(La) and 2.994, 2.77 and 2.73 Å, respectively, in radekškodaite-(Ce): see below the description of their crystal structures). Bands in the 1000–1100 cm^{-1} range correspond to stretching vibrations of the Si–O–Si fragments in Si_2O_7 groups, those in 850–1000 cm^{-1} region are due to stretching vibrations of apical Si–O bonds, and those in 650–690 cm^{-1} area to Al–O···H bending vibrations. Bands in the 290–630 cm^{-1} range correspond to mixed modes and overlapping bands of (Al,Fe^{3+},Mg)–O stretching vibrations, as well as bending vibrations of silicate groups, while those with frequencies below 300 cm^{-1} correspond to lattice modes involving *REE*–O, Ca–O and Fe^{2+}–O stretching vibrations and librational vibrations of silicate groups.

The Raman spectra of both new minerals are close to those of västmanlandite-(Ce) (Holtstam *et al.*, 2005) and ferriperbøeite-(La) (Kasatkin *et al.*, 2020b) in the range of 300–1000 cm^{-1} but significantly differ from them in the regions of stretching vibrations of the Si–O–Si fragments (1000 to 1100 cm^{-1}), O–H stretching vibrations (above 3200 cm^{-1}) and stretching vibrations involving *REE* and bivalent cations forming low-force-strength bonds (below 300 cm^{-1}). In particular, in the spectra of radekškodaite-(La) and radekškodaite-(Ce), the vibrational bands of stretching vibrations of the Si–O–Si fragments are significantly weaker than in the ferriperbøeite-(La) spectrum, which reflects a lower Si_2O_7:SiO_4 ratio in their composition.

The band at 687 cm^{-1} in the Raman spectrum of radekškodaite-(La) and the one at 690 cm^{-1} in the Raman spectrum of radekškodaite-(Ce) are close to the strong band in the Raman spectrum of allanite-(Ce) 689 cm^{-1} (Andò and Garzanti, 2014; Č3) and can be tentatively assigned to the epidote-type module.

Chemical composition

Chemical data for both new minerals were obtained using a Cameca SX-100 electron microprobe (WDS mode, acceleration voltage of 15 kV, a beam current of 20 nA and a 3 μm beam

https://doi.org/10.1180/mgm.2020.64 Published online by Cambridge University Press

diameter). The spectral interference of F*K*α and Ce*M*ζ were manually corrected using empirically determined correction factors. H_2O was not determined directly due to the scarcity of pure material and was calculated by stoichiometry on the basis of $O_{28}(OH,F)_3$ taking into account that bond-valence sums for the O(1), O(2) and O(3) sites are close to 1 (see below). Both the crystal structure and Raman spectroscopy data confirm the presence of OH groups and the absence of carbonate and borate groups in both new species. Attempts to determine the valence state of iron using Mössbauer spectroscopy were unsuccessful due to a lack of pure material: small but abundant inclusions of allanite–ferriallanite and ferriperbøeite-(La) in radekškodaite-(La) and those of perbøeite-(Ce) in radekškodaite-(Ce) significantly affect the reliability of the data. For this reason, the Fe^{3+}:Fe^{2+} ratio was determined on the basis of the charge balance requirement.

Analytical data are given in Table 2. Contents of other elements with atomic numbers higher than that of carbon are below detection limits.

The empirical formulae calculated on the basis of $O_{28}(OH,F)_3$ are: radekškodaite-(La), $(Ca_{0.98}Th_{0.01}La_{2.75}Ce_{2.01}Nd_{0.16}Pr_{0.09})_{\Sigma 6.00}(Al_{3.28}Fe^{3+}_{0.63}Fe^{2+}_{0.57}Mg_{0.34}Mn_{0.15}Ti_{0.03})_{\Sigma 5.00}Si_{7.00}O_{28}[(OH)_{2.91}F_{0.09}]$; and radekškodaite-(Ce), $(Ca_{0.79}Mn_{0.16}Th_{0.01}Ce_{2.39}La_{2.20}Nd_{0.30}Pr_{0.14})_{\Sigma 5.99}(Al_{3.43}Fe^{2+}_{0.62}Fe^{3+}_{0.52}Mg_{0.42}Ti_{0.01})_{\Sigma 5.00}Si_{7.00}O_{28}[(OH)_{2.92}F_{0.08}]$.

The idealised formulae are as follows. Radekškodaite-(La): $(CaLa_5)(Al_4Fe^{2+})[Si_2O_7][SiO_4]_5O(OH)_3$ which requires CaO 3.52, FeO 4.50, La_2O_3 51.11, Al_2O_3 12.79, SiO_2 26.38, H_2O 1.70, total 100 wt.%. Radekškodaite-(Ce): $(CaCe_5)(Al_4Fe^{2+})[Si_2O_7][SiO_4]_5O(OH)_3$ which requires CaO 3.50, FeO 4.49, Ce_2O_3 51.29, Al_2O_3 12.75, SiO_2 26.28, H_2O 1.69, total 100 wt.%.

X-ray crystallography

Powder XRD data for radekškodaite-(La) (Table 3) were collected with a Rigaku R-AXIS Rapid II single-crystal diffractometer equipped with a cylindrical image plate detector (radius 127.4 mm) using Debye-Scherrer geometry, Co*K*α radiation (rotating anode with VariMAX microfocus optics), 40 kV, 15 mA and exposure of 15 min. Angular resolution of the detector is 0.045°2θ (pixel size is 0.1 mm). The data were integrated using the software package *Osc2Tab* (Britvin *et al.*, 2017). The powder XRD data for radekškodaite-(Ce) (Table 4) were collected with a Supernova Rigaku-Oxford Diffraction diffractometer equipped with a Pilatus 200 K Dectris detector and an X-ray micro-source (Mo*K*α radiation) with spot size of ~0.12 mm. The detector-to-sample distance was 68 mm. Data reduction was performed using *CrysAlis*^{Pro} (Rigaku-Oxford Diffraction). A standard phi scan mode as implemented in the powder power tool of *CrysAlis*^{Pro} was used for the powder data collection. Parameters of monoclinic unit cells refined from the powder data are for radekškodaite-(La): $a = 8.958(6)$, $b = 5.730(3)$, $c = 25.13(2)$ Å, $\beta = 116.68(5)°$ and $V = 1153(2)$ Å^3; and for radekškodaite-(Ce): $a = 8.9982(6)$, $b = 5.6720(4)$, $c = 25.192(2)$ Å, $\beta = 116.912(9)°$ and $V = 1146.5(2)$ Å^3.

Single-crystal X-ray studies of both new minerals were carried out using an Xcalibur S diffractometer equipped with a CCD detector for grains analysed by electron microprobe and then extracted from the polished sections. A full sphere of three-dimensional data was collected. Data reduction was performed using *CrysAlis*^{Pro} *Version 1.171.37.35* (Agilent Technologies, 2014). The data were corrected for Lorentz factor and polarisation effects.

The crystal structure of radekškodaite-(La) was solved by direct methods and refined with the use of the *SHELX-97* software package (Sheldrick, 2008) to $R = 0.0554$ for 2837 unique reflections with $I > 2\sigma(I)$. The crystal structure of radekškodaite-(Ce) was refined with a model of radekškodaite-(La) as the starting one and using the *SHELX* software package (Sheldrick, 2015) to $R = 0.0769$ for 3050 unique reflections with $I > 2\sigma(I)$. The H atoms of the OH groups of both minerals were located from the difference-Fourier synthesis and their positions were restricted to keep O–H distances of 0.85(1) Å.

The crystal data, data collection information and structure refinement details for radekškodaite-(La) and radekškodaite-

Table 2. Average chemical composition of radekškodaite-(La) and radekškodaite-(Ce) (wt.%).

	Radekškodaite-(La)			Radekškodaite-(Ce)			
Constituent	Mean, *n* = 7	Range	S.D.	Mean, *n* = 7	Range	S.D.	Probe standard
CaO	3.40	3.33–3.44	0.04	2.74	2.57–3.08	0.21	Wollastonite
La_2O_3	27.68	26.83–28.78	0.61	22.23	21.79–22.78	0.44	$LaPO_4$
Ce_2O_3	20.39	20.16–20.62	0.16	24.30	24.19–24.35	0.07	$CePO_4$
Pr_2O_3	0.94	0.85–1.05	0.09	1.48	1.47–1.49	0.01	$PrPO_4$
Nd_2O_3	1.71	1.63–1.82	0.07	3.18	3.08–3.29	0.09	$NdPO_4$
ThO_2	0.23	0.16–0.28	0.04	0.24	0.20–0.35	0.06	$CaTh(PO_4)_2$
MgO	0.85	0.77–1.05	0.10	1.04	0.97–1.11	0.06	Mg_2SiO_4
Al_2O_3	10.35	9.99–10.58	0.22	10.84	10.71–10.96	0.09	Sanidine
MnO	0.64	0.58–0.71	0.04	0.69	0.55–0.73	0.08	Spessartine
FeO*	2.55	5.15–5.88**	0.25**	2.76	4.41–5.51**	0.47**	Almandine
Fe_2O_3*	3.12			2.57			
TiO_2	0.13	0.08–0.20	0.05	0.04	0.00–0.06	0.03	Anatase
SiO_2	26.03	25.30–26.51	0.36	26.10	24.78–26.81	0.90	Sanidine
F	0.10	0.07–0.15	0.03	0.09	0.06–0.11	0.02	Topaz
H_2O***	1.62			1.63			
–O=F	–0.04			–0.04			
Total	99.70			99.89			

S.D. = standard deviation.
*Apportioned from total Fe measured as FeO content of 5.36 wt.% for radekškodaite-(La) and 5.07 wt.% for radekškodaite-(Ce) in accordance with bond-valence sums for the cationic sites and charge-balance requirement for the empirical formulae.
**For total iron calculated as FeO.
***Calculated by stoichiometry.

https://doi.org/10.1180/mgm.2020.64 Published online by Cambridge University Press

Table 3. Powder X-ray diffraction data for radekškodaite-(La).

I_{obs}	I_{calc}*	d_{obs}	d_{calc}**	*h k l*
52	58	**22.1**	22.449	001
9	8	11.26	11.225	002
32	19	8.01	8.010	100
5	2	7.51	7.483	003
9	7	7.33	7.354	$\bar{1}03$
65	36	**4.661**	4.658	110
10	7, 6	4.543	4.547, 4.546	013, 103
8	1, 4	4.477	4.490, 4.459	005, $\bar{2}03$
14	4, 4	4.008	4.008, 4.005	014, 200
6	2, 4	3.752	3.759, 3.741	$\bar{1}15$, 006
78	2, 1, 40	**3.522**	3.560, 3.533, 3.518	113, 015, $\bar{2}.2.13$
12	5	3.440	3.436	$\bar{2}14$
23	1, 10	3.287	3.286, 3.282	$\bar{2}15$, 210
8	3, 6	3.203	3.207, 3.198	007, 114
3	2	3.131	3.132	016
55	100	**3.038**	3.037	$\bar{1}17$
45	18, 5	**3.010**	3.014, 2.985	203, $\bar{3}04$
44	43	**2.866**	2.863	020
15	1, 28	2.801	2.803, 2.798	$\bar{3}01$, 017
42	28	**2.732**	2.732	204
20	17	2.687	2.696	120
100	7, 59	**2.640**	2.647, 2.637	$\bar{3}14$, $\bar{3}13$
5	2	2.565	2.561	$\bar{3}16$
10	12	2.479	2.475	$\bar{3}17$
3	4	2.423	2.423	123
5	3	2.367	2.369	117
4	2	2.335	2.331	$\bar{2}25$
8	4	2.281	2.285	$\bar{2}.1.10$
13	11	2.259	2.259	$\bar{2}26$
6	5	2.242	2.245	0.0.10
17	2, 15	2.195	2.198, 2.196	$\bar{4}07$, $\bar{4}03$
20	26, 2	2.176	2.173, 2.171	$\bar{2}27$, 222
10	9	2.136	2.136	027
14	4, 5	2.097	2.090, 2.088	0.1.10, 207
10	17	2.078	2.076	223
6	21	1.978	1.977	224
18	12	1.958	1.952	314
9	5	1.936	1.931	$\bar{2}.0.13$
10	5	1.895	1.894	$\bar{4}.1.10$
9	3, 5	1.885	1.890, 1.880	410, $\bar{2}.2.10$
8	2, 4	1.860	1.870, 1.857	$\bar{1}.0.13$, 130
15	16	1.846	1.843	1.1.10
11	4, 4, 6, 4	1.794	1.793, 1.792, 1.791, 1.791	$\bar{3}.2.10$, 506, $\bar{2}.0.14$, $\bar{3}.1.13$
6	5	1.764	1.767	0.2.10
5	7	1.745	1.742	$\bar{4}23$
3	8	1.712	1.712	1.1.11
7	13, 3	1.682	1.685, 1.681	$\bar{1}37$, 324
10	3, 1, 7	1.661	1.666, 1.662, 1.659	2.0.10, 0.2.11, $\bar{5}13$
16	4, 16, 1, 5	1.644	1.646, 1.643, 1.641, 1.640	$\bar{5}.1.10$, $\bar{4}.2.10$, 420, 037
13	12, 1, 2	1.605	1.606, 1.604, 1.602	$\bar{3}33$, 0.0.14, 500
7	1, 3	1.543	1.544, 1.543	0.1.14, 510
4	7	1.520	1.519	$\bar{2}.2.14$
4	3	1.501	1.503	2.1.11
7	3, 3, 4	1.475	1.480, 1.474, 1.473	$\bar{1}.2.14$, $\bar{6}.0.10$, $\bar{5}.2.10$
12	7, 3, 4, 13	1.435	1.439, 1.438, 1.434, 1.432	424, $\bar{6}16$, 407, 040
4	1, 6, 2	1.395	1.398, 1.394, 1.391	520, $\bar{4}.1.17$, 417

*For the calculated pattern, only reflections with intensities ≥1 are given.
**For the unit-cell parameters calculated from single-crystal data.
The eight strongest reflections are given in boldtype.

(Ce) are given in Table 5, atomic coordinates, thermal displacement parameters of atoms and site occupancies in Table 6, selected interatomic distances in Table 7 and hydrogen bonds in Table 8. Bond-valence calculations are given in Table 9. The crystallographic information files for both minerals have been deposited with the Principal Editor of *Mineralogical Magazine* and are available as Supplementary material (see below).

Table 4. Powder X-ray diffraction data for radekškodaite-(Ce).

I_{obs}	I_{calc}*	d_{obs}	d_{calc}**	*h k l*
38	56	**22.5**	22.468	001
9	8	11.27	11.234	002
42	20	**8.08**	8.009	100
18	7	7.43	7.372	$\bar{1}03$
76	41	**4.640**	4.646	110
24	5	4.331	4.331	111
10	5	4.009	4.000	200
12	4	3.724	3.745	006
99	42	**3.528**	3.516	$\bar{2}13$
9	5	3.403	3.435	$\bar{2}14$
35	18	3.305	3.379	$\bar{1}16$
100	100	**3.031**	3.038	$\bar{1}17$
46	43	**2.844**	2.852	020
18	28	2.734	2.731	204
87	57	**2.654**	2.637	$\bar{3}13$
16	12	2.491	2.477	$\bar{3}17$
9	9	2.318	2.318	$\bar{3}.0.10$
12	11	2.265	2.256	$\bar{2}26$
35	27	2.184	2.170	$\bar{2}27$
37	17	**2.073**	2.071	223
29	20	1.967	1.972	224
11	6	1.886	1.896	$\bar{4}.1.10$
16	16	1.846	1.843	1.1.10
14	6	1.802	1.795	$\bar{2}.0.14$
18	7	1.738	1.740	$\bar{4}23$
22	13	1.659	1.680	$\bar{1}37$
15	11	1.602	1.602	$\bar{3}33$
4	6	1.520	1.519	$\bar{2}.2.14$
13	6	1.432	1.437	424
3	2	1.368	1.369	$\bar{1}.1.17$

*For the calculated pattern, only reflections with intensities ≥1 are given.
**These data were calculated from the structure determined by single-crystal X-ray data.
The eight strongest reflections are given in boldtype.

Crystal structure

Radekškodaite-(La) and radekškodaite-(Ce) are isostructural and, thus there is one crystal-structure diagram (Fig. 6) for both minerals. They belong to a new structure type related to the members of the recently approved gatelite supergroup (Bonazzi *et al.*, 2019). The latter are considered as iso-topological **ET** type polysomes within a polysomatic series which has epidote-type and törnebohmite-type structures as end-members (Shen and Moore, 1982). Their structures can be described as a regular alternating 1:1 stacking of slabs with the epidote-type structure (E) and slabs with the törnebohmite-type structure (T) (Bonazzi *et al.*, 2003, 2014; Holtstam *et al.*, 2005; Bindi *et al.*, 2018). In the radekškodaite structure, regular alternation of one epidote-type module with two törnebohmite-type modules is observed. This results in the formation of a new polysome that we propose to name the **ET2** type. The abbreviations of the structural sites in the text below are given in accordance with the above mentioned nomenclature of gatelite-supergroup minerals where the *A* sites are occupied by cations in large cavities, mainly Ca and *REE*, and the *M* sites have octahedral coordination and are occupied by di- and trivalent cations, namely Al, Fe^{2+}, Fe^{3+}, Mg, Mn^{2+} and Mn^{3+}. (Bonazzi *et al.*, 2019).

The crystal structure of radekškodaite consists of chains of edge-sharing octahedra running along the **b** axis: single chains of the *M*(2)- and *M*(4)-centred octahedra and branched chains with the *M*(1)-centred octahedra in the central part with the *M*(3)-centred octahedra attached to them from both sides. The chains are linked *via* isolated $[SiO_4]$ tetrahedra and disilicate

https://doi.org/10.1180/mgm.2020.64 Published online by Cambridge University Press

Table 5. Crystal data, data collection information and structure refinement details for radekškodaite-(La) and radekškodaite-(Ce).

Crystal data		
Mineral	Radekškodaite-(La)	Radekškodaite-(Ce)
Formula	$^{A1}(Ca_{0.96}LREE_{0.04})^{A2-6}LREE_5$ $^{M1}(Al_{0.49}Fe^{3+}_{0.36}Mg_{0.15})^{M2}(Al_{1.88}Fe^{3+}_{0.12})$ $^{M3}(Fe^{2+}_{0.57}Mg_{0.18}Mn_{0.14}Fe^{3+}_{0.11})^{M4}(Al_{0.93}Fe^{3+}_{0.07})$ $[Si_2O_7][SiO_4]_5O(OH)_3$	$^{A1}(Ca_{0.79}Mn_{0.16}LREE_{0.05})^{A2-6}LREE_5$ $^{M1}(Al_{0.62}Fe^{3+}_{0.23}Mg_{0.15})^{M2}(Al_{1.89}Fe^{3+}_{0.11})$ $^{M3}(Fe^{2+}_{0.63}Mg_{0.27}Fe^{3+}_{0.10})^{M4}(Al_{0.93}Fe^{3+}_{0.07})$ $[Si_2O_7][SiO_4]_5O(OH)_3$
Formula weight	1614.42	1610.40
Crystal size (mm)	0.04 × 0.11 × 0.16	0.10 × 0.22 × 0.31
Temperature (K)	293(2)	293(2)
Crystal system, space group, *Z*	Monoclinic, $P2_1/m$, 2	Monoclinic, $P2_1/m$, 2
Unit cell dimensions (Å/°)	*a* = 8.9604(3), *b* = 5.7268(2), *c* = 25.1128(10) β = 116.627(5)	*a* = 8.9702(4), *b* = 5.7044(2), *c* = 25.1642(13) β = 116.766(6)
V (Å^3)	1151.98(7)	1149.68(11)
Absorption coefficient μ, (mm^{-1})	11.45	11.41
F_{000}	1486	1482
Data collection		
Diffractometer	Xcalibur S CCD	Xcalibur S CCD
Radiation and wavelength (Å)	Mo*Kα*; 0.71073	Mo*Kα*; 0.71073
Data reduction	CrysAlis^{Pro}, Agilent Technologies, Version 1.171.37.34 (Agilent Technologies, 2014)	CrysAlis^{Pro}, Agilent Technologies, Version 1.171.37.34 (Agilent Technologies, 2014)
Absorption correction	Gaussian	Gaussian
	Numerical absorption correction based on Gaussian integration over a multifaceted crystal model. Empirical absorption correction using spherical harmonics, implemented in *SCALE3 ABSPACK* scaling algorithm.	
θ range (°)	2.72–28.28	3.061–28.28
Reflections collected	20,205	20,324
Unique reflections	3130 (R_{int} = 0.0544)	3122 (R_{int} = 0.0429)
Unique reflections with $I > 2\sigma(I)$	2837	3050
Index ranges	$-11 \leq h \leq 11$, $-7 \leq k \leq 7$, $-33 \leq l \leq 33$	$-11 \leq h \leq 11$, $-7 \leq k \leq 7$, $-33 \leq l \leq 33$
Refinement		
Structure solution	Direct methods	Refined crystal structure of radekškodaite-(La) was used as initial model
Refinement method	Full-matrix least-squares on F^2	Full-matrix least-squares on F2
Number of refined parameters	289	282
Final *R* indices [$I > 2\sigma(I)$]	R_1 = 0.0554, wR_2* = 0.1089	R_1 = 0.0769, wR_2* = 0.1471
R indices (all data)	R_1 = 0.0636, wR_2* = 0.1123	R_1 = 0.0783, wR_2* = 0.1476
GoF	1.221	1.334
Largest diff. peak and hole, (e^-/Å^3)	2.69 and −2.13	2.58 and −4.28

*$w = 1/[\sigma^2(F_o^2) + (0.0391P)^2 + 14.1116P]$; $P = \{[\text{max of } (0 \text{ or } F_o^2)] + 2F_c^2\}/3$ for radekškodaite-(La)
$w = 1/[\sigma^2(F_o^2) + (0.0165P)^2 + 72.0691P]$; $P = \{[\text{max of } (0 \text{ or } F_o^2)] + 2F_c^2\}/3$ for radekškodaite-(Ce)

groups $[Si_2O_7]$. The *A*(1–6) sites occur in large cavities. The Si–O–Si angles in the disilicate groups of both species are very close to each other: 148.9(6)° in radekškodaite-(La) and 149.0(13)° in radekškodaite-(Ce) (Table 7).

Despite La^{3+} being a dominant *REE* in radekškodaite-(La), the Ce^{3+} scattering curve was used during the structure refinement for the *A*(1–6) sites of both new minerals because of the significant [dominant in radekškodaite-(Ce)] content of Ce^{3+} cations, minor amounts of heavier Nd^{3+} and Pr^{3+}, and very minor amounts of Th^{4+}.

According to the site-occupancy factors refinement and cation–anion distances (Table 7), the *A*(2–6) sites are occupied by *REE* cations. The refinement of their site occupancy factors gave the values very close to 1.0 and thus according to chemical data and the results of the refinement these sites are considered as fully occupied by *REE* cations. The *A*(1) site in both species is Ca dominant with minor *REE* admixture. In radekškodaite-(La) the refined *A*(1) site population is $Ca_{0.955(5)}LREE_{0.045(5)}$, where *LREE* implies light rare earth elements. Thus, the total composition of the *A* sites in radekškodaite-(La) is $LREE_{5.04}Ca_{0.96}$, which is in a good agreement with the electron microprobe data (Table 2). In radekškodaite-(Ce) we also assume some Mn occupies the *A*(1) site due to the lack of cations at *A* sites and excess of cations at octahedral *M* sites, but we do not exclude that minor Mn may also occupy the *M*(3) site. For the *A*(1) site, Ca *vs.* Ce was refined (e_{ref} = 22.89), and on the basis of chemical data and e_{ref}, the *A*(1) site was assumed to be occupied by Ca, Mn and *REE* in the ratio 0.79:0.16:0.05 (e_{calc} = 22.70). Thus, the total composition of the *A* sites in radekškodaite-(Ce) is $LREE_{5.05}Ca_{0.79}Mn_{0.16}$, which is also in a good agreement with the electron microprobe data (Table 2).

There are four octahedral *M* sites, *M*(1–4). For the *M*(1), *M*(2) and *M*(4) sites, Al *vs.* Fe was refined, and for the *M*(3) site, Fe *vs.* Mg was refined. The *M*(1), *M*(2) and *M*(4) sites are Al-dominant. The refined population of the *M*(2) and *M*(4) sites is $Al_{0.939(10)}Fe_{0.061(10)}$ / $Al_{0.926(14)}Fe_{0.074(14)}$, respectively, in radekškodaite-(La) and $Al_{0.945(16)}Fe_{0.055(16)}$ / $Al_{0.93(2)}Fe_{0.07(2)}$, respectively, in radekškodaite-(Ce). These sites centre the smallest octahedra with the mean distances of 1.915 Å [*M*(2)–O] and 1.916 Å [*M*(4)–O] in radekškodaite-(La) and 1.914 Å [*M*(2)–O] and 1.908 Å [*M*(4)–O] in radekškodaite-(Ce). The *M*(1)-centred octahedron is slightly larger, with the mean *M*(1)–O distance in radekškodaite-(La)/radekškodaite-(Ce) of 1.975/1.965 Å and the refined number of electrons (e_{ref}) at the *M*(1) site being 17.50/15.86. This site is assumed to be occupied predominantly by Al with subordinate Fe^{3+} and Mg cations in the ratio Al:Fe^{3+}:Mg equal to 0.49:0.36:0.15 in radekškodaite-(La) and 0.62:0.23:0.15 in radekškodaite-(Ce). The largest *M*(3) octahedron with the mean *M*(3)–O distance of 2.146/2.111 Å is predominately occupied by Fe^{2+} with subordinate Mg, Mn and Fe^{3+} in radekškodaite-(La) and by Mg and Fe^{3+} in radekškodaite-(Ce). According to electron microprobe data and the refined number of electrons in radekškodaite-(La)/

https://doi.org/10.1180/mgm.2020.64 Published online by Cambridge University Press

Table 6. Coordinates, equivalent displacement parameters (U_{eq}, in Å^2) and anisotropic displacement parameters of atoms (excepting H) and site occupancy factors (s.o.f.) for radekškodaite-(La) and radekškodaite-(Ce).

Site	*x*	*y*	*z*	U_{eq}	s.o.f.	U^{11}	U^{22}	U^{33}	U^{23}	U^{13}	U^{12}
Radekškodaite-(La)											
A(1)	0.2275(3)	¾	−0.06427(10)	0.0177(8)	$Ca_{0.955(5)}LREE_{0.045(5)}$	0.0231(14)	0.0155(13)	0.0192(13)	0.000	0.0138(10)	0.000
A(2)	0.59128(8)	¼	0.47053(3)	0.01369(16)	$LREE_{1.00}$	0.0092(3)	0.0196(3)	0.0097(3)	0.000	0.0018(2)	0.000
A(3)	0.43193(8)	¾	0.23650(3)	0.01402(17)	$LREE_{1.00}$	0.0111(3)	0.0170(3)	0.0123(3)	0.000	0.0037(2)	0.000
A(4)	0.61439(8)	¼	0.17665(3)	0.01432(17)	$LREE_{1.00}$	0.0107(3)	0.0178(4)	0.0123(3)	0.000	0.0033(2)	0.000
A(5)	0.77054(10)	¼	0.34757(3)	0.0344(2)	$LREE_{1.00}$	0.0181(4)	0.0711(7)	0.0101(3)	0.000	0.0027(3)	0.000
A(6)	0.75187(10)	¼	0.64030(3)	0.0285(2)	$LREE_{1.00}$	0.0195(4)	0.0522(6)	0.0097(3)	0.000	0.0029(3)	0.000
M(1)	0.0	½	0.0	0.0098(5)	$Al_{0.49}Fe_{0.36}Mg_{0.15}$*	0.0078(11)	0.0086(11)	0.0130(11)	0.0012(9)	0.0047(9)	−0.0004(9)
M(2)	0.0280(3)	0.4995(4)	0.20866(10)	0.0113(7)	$Al_{0.939(10)}Fe_{0.061(10)}$	0.0090(12)	0.0102(12)	0.0143(12)	−0.0008(9)	0.0050(9)	0.0001(8)
M(3)	0.3126(2)	¾	0.08710(8)	0.0140(4)	$Fe_{0.68}Mg_{0.18}Mn_{0.14}$*	0.0109(9)	0.0115(9)	0.0140(9)	0.000	0.0007(7)	0.000
M(4)	0.0	½	½	0.0117(10)	$Al_{0.926(14)}Fe_{0.074(14)}$	0.0074(16)	0.0101(17)	0.0151(17)	0.0001(12)	0.0027(12)	−0.0008(12)
Si(1)	0.2018(4)	¼	0.13317(13)	0.0081(6)	$Si_{1.00}$	0.0068(14)	0.0078(14)	0.0100(14)	0.000	0.0040(11)	0.000
Si(2)	0.3557(4)	¼	0.29804(13)	0.0076(6)	$Si_{1.00}$	0.0057(14)	0.0067(14)	0.0089(13)	0.000	0.0021(11)	0.000
Si(3)	0.7028(4)	¾	0.11704(13)	0.0090(6)	$Si_{1.00}$	0.0067(14)	0.0072(14)	0.0108(14)	0.000	0.0019(11)	0.000
Si(4)	0.8397(4)	¾	0.28053(14)	0.0117(6)	$Si_{1.00}$	0.0099(15)	0.0132(16)	0.0124(15)	0.000	0.0053(12)	0.000
Si(5)	0.6709(4)	¾	0.40930(13)	0.0086(6)	$Si_{1.00}$	0.0061(13)	0.0073(14)	0.0107(14)	0.000	0.0024(11)	0.000
Si(6)	0.1817(4)	¼	0.42582(13)	0.0102(6)	$Si_{1.00}$	0.0080(14)	0.0112(15)	0.0101(14)	0.000	0.0028(12)	0.000
Si(7)	0.3419(4)	¼	0.01496(13)	0.0088(6)	$Si_{1.00}$	0.0091(14)	0.0045(14)	0.0099(14)	0.000	0.0018(11)	0.000
O(1)	0.9251(9)	¼	0.5300(3)	0.0110(16)	$O_{1.00}$	0.006(4)	0.013(4)	0.011(4)	0.000	0.002(3)	0.000
H(1)	0.980(18)	¼	0.5678(8)	0.04(5)**	$H_{1.00}$						
O(2)	0.1053(10)	¾	0.1785(4)	0.0118(16)	$O_{1.00}$	0.008(4)	0.009(4)	0.016(4)	0.000	0.004(3)	0.000
H(2)	0.08(3)	¾	0.141(2)	0.10(9)**	$H_{1.00}$						
O(3)	0.9499(10)	¼	0.2384(3)	0.0121(16)	$O_{1.00}$	0.014(4)	0.015(4)	0.004(3)	0.000	0.000(3)	0.000
H(3)	1.000(18)	¼	0.2762(6)	0.04(5)**	$H_{1.00}$						
O(4)	0.0613(10)	¾	0.0541(4)	0.0163(18)	$O_{1.00}$	0.015(4)	0.014(4)	0.016(4)	0.000	0.003(3)	0.000
O(5)	0.5828(14)	¾	0.3384(4)	0.038(3)	$O_{1.00}$	0.038(6)	0.059(8)	0.009(4)	0.000	0.003(4)	0.000
O(6)	0.2385(7)	0.4895(10)	0.0119(3)	0.0171(12)	$O_{1.00}$	0.018(3)	0.010(3)	0.025(3)	0.003(2)	0.010(3)	0.002(2)
O(7)	0.3740(11)	¼	−0.0442(4)	0.022(2)	$O_{1.00}$	0.022(5)	0.033(6)	0.013(4)	0.000	0.009(4)	0.000
O(8)	0.4845(11)	¼	0.2694(4)	0.026(2)	$O_{1.00}$	0.012(4)	0.045(6)	0.024(5)	0.000	0.010(4)	0.000
O(9)	0.0571(10)	¼	0.4589(4)	0.0134(17)	$O_{1.00}$	0.009(4)	0.012(4)	0.020(4)	0.000	0.007(3)	0.000
O(10)	0.9695(9)	¾	0.2492(4)	0.0120(16)	$O_{1.00}$	0.007(4)	0.012(4)	0.018(4)	0.000	0.007(3)	0.000
O(11)	0.0920(10)	¼	0.1709(3)	0.0113(16)	$O_{1.00}$	0.015(4)	0.008(4)	0.018(4)	0.000	0.013(3)	0.000
O(12)	0.3044(8)	0.4756(10)	0.4439(3)	0.0192(13)	$O_{1.00}$	0.021(3)	0.008(3)	0.037(4)	−0.003(3)	0.020(3)	−0.003(2)
O(13)	0.8139(7)	0.5132(10)	0.1424(2)	0.0133(11)	$O_{1.00}$	0.012(3)	0.006(3)	0.016(3)	−0.001(2)	0.001(2)	0.001(2)
O(14)	0.3269(7)	0.4734(10)	0.1485(2)	0.0128(11)	$O_{1.00}$	0.011(3)	0.014(3)	0.012(3)	−0.003(2)	0.004(2)	−0.004(2)
O(15)	0.7842(7)	0.5121(10)	0.4334(3)	0.0149(12)	$O_{1.00}$	0.010(3)	0.011(3)	0.020(3)	0.001(2)	0.003(2)	0.002(2)
O(16)	0.7166(7)	0.5243(10)	0.2607(3)	0.0180(13)	$O_{1.00}$	0.022(3)	0.007(3)	0.032(3)	−0.002(2)	0.019(3)	−0.003(2)
O(17)	0.0543(10)	¼	0.0630(3)	0.0131(16)	$O_{1.00}$	0.010(4)	0.013(4)	0.011(4)	0.000	0.000(3)	0.000
O(18)	0.2431(7)	0.4889(10)	0.2762(3)	0.0138(12)	$O_{1.00}$	0.008(3)	0.006(3)	0.021(3)	−0.001(2)	0.001(2)	0.000(2)
O(19)	0.5225(10)	¼	0.0717(3)	0.0130(16)	$O_{1.00}$	0.011(4)	0.013(4)	0.009(4)	0.000	−0.001(3)	0.000
O(20)	0.5581(11)	¾	0.1375(4)	0.026(2)	$O_{1.00}$	0.020(5)	0.045(6)	0.024(5)	0.000	0.020(4)	0.000
O(21)	0.4574(14)	¼	0.3682(4)	0.040(3)	$O_{1.00}$	0.037(6)	0.060(8)	0.006(4)	0.000	−0.005(4)	0.000
O(22)	0.5371(12)	¾	0.4353(4)	0.031(2)	$O_{1.00}$	0.015(5)	0.058(7)	0.023(5)	0.000	0.011(4)	0.000
O(23)	0.0596(14)	0.3198(18)	0.3568(5)	0.015(3)	$O_{0.50}$	0.019(6)	0.010(6)	0.010(5)	0.001(4)	0.001(4)	−0.001(4)
O(24)	0.9565(14)	0.8163(17)	0.3507(5)	0.014(3)	$O_{0.50}$	0.021(6)	0.004(6)	0.012(5)	−0.002(4)	0.004(4)	−0.003(4)

(*Continued*)

radekškodaite-(Ce) (e_{ref} = 23.40/22.22), the atomic ratio in the former is Fe^{2+}:Mg:Mn:Fe^{3+} = 0.57:0.18:0.14:0.11, while in the latter it is Fe^{2+}:Mg:Fe^{3+} = 0.63:0.27:0.10. During the refinement, splitting was found for the O(23) and O(24) sites which deviate from the *m* plane just as it does in the structures of gatelite-supergroup minerals. Bond-valence calculations (Table 9) confirm the above conclusions about distribution of cations between different sites.

Discussion

As noted above, the structures of both new minerals can be described as a regular alternating 1:2 stacking of slabs of epidote-type (**E**) and törnebohmite-type (**T**) structures (Fig. 6). The **E** modules are (001) slabs with the allanite composition Ca*REE*$Al_2Fe^{2+}[Si_2O_7][SiO_4]X$(OH), where $X = O^{2-}$ and/or F^-. The **T** modules are ($\bar{1}$02) slabs with the törnebohmite composition [$REE_2Al(SiO_4)_2$(OH)].

Commonly, the *REE* nodules from Mochalin Log show concentric texture. The arrangement of the mineral assemblage follows a trend of decreasing *REE* content in minerals from the core to the rim of the nodule. A similar feature was observed in monazite replaced by allanite and *REE*-enriched epidote during metamorphism in metapelites (Finger *et al.*, 1998), in magmatic *REE*-rich accumulations from aplitic rock at Jamestown, Colorado (Allaz *et al.*, 2015) and locally in the Bästnas-type deposits in Bergslagen, Sweden (e.g. Andersson, 2004). The most *REE*-enriched minerals occurring in central parts of the described nodules from Mochalin Log include bastnäsite, britholite, percleveite and torneböhmite, whereas the occurrence of *REE*-enriched epidote-supergroup members and structurally related silicates is confined to the outermost parts. The following generalised mineral sequence of torneböhmite–epidote polysomatic series from the core of the nodules to their rims is documented: torneböhmite → radekškodaite → perbøeite (ferriperbøeite) → allanite (ferriallanite) → *REE*-enriched

https://doi.org/10.1180/mgm.2020.64 Published online by Cambridge University Press

Table 6. (*Continued.*)

Site	*x*	*y*	*z*	U_{eq}	s.o.f.	U^{11}	U^{22}	U^{33}	U^{23}	U^{13}	U^{12}
Radekškodaite-(Ce)											
A(1)	0.2294(5)	¾	−0.06411(16)	0.0224(7)	$Ca_{0.79}Mn_{0.16}LREE_{0.05}$*	0.0317(18)	0.0220(18)	0.0229(16)	0.000	0.0207(15)	0.000
A(2)	0.59226(13)	¼	0.47016(4)	0.0156(2)	$LREE_{1.00}$	0.0115(5)	0.0225(6)	0.0097(4)	0.000	0.0019(4)	0.000
A(3)	0.43061(13)	¾	0.23681(5)	0.0159(2)	$LREE_{1.00}$	0.0139(5)	0.0188(5)	0.0134(5)	0.000	0.0049(4)	0.000
A(4)	0.61611(13)	¼	0.17623(5)	0.0175(2)	$LREE_{1.00}$	0.0152(5)	0.0189(6)	0.0147(5)	0.000	0.0036(4)	0.000
A(5)	0.77126(16)	¼	0.34738(5)	0.0364(4)	$LREE_{1.00}$	0.0220(6)	0.0719(12)	0.0111(5)	0.000	0.0036(4)	0.000
A(6)	0.75300(16)	¼	0.64028(5)	0.0308(3)	$LREE_{1.00}$	0.0228(6)	0.0549(9)	0.0095(5)	0.000	0.0027(4)	0.000
M(1)	0.0	½	0.0	0.0101(8)	$Al_{0.62}Fe_{0.23}Mg_{0.15}$*	0.0101(17)	0.0048(19)	0.0143(18)	0.0000(15)	0.0046(15)	−0.0016(15)
M(2)	0.0280(4)	0.4995(7)	0.20823(15)	0.0113(11)	$Al_{0.945(16)}Fe_{0.055(16)}$	0.0082(17)	0.0100(18)	0.0149(18)	−0.0008(13)	0.0045(13)	0.0003(13)
M(3)	0.3124(4)	¾	0.08697(14)	0.0194(12)	$Fe_{0.73(2)}Mg_{0.27(2)}$	0.0171(18)	0.0172(19)	0.0121(16)	0.000	−0.0037(12)	0.000
M(4)	0.0	½	½	0.0142(16)	$Al_{0.93(2)}Fe_{0.07(2)}$	0.011(2)	0.010(3)	0.018(3)	0.0017(19)	0.0028(19)	−0.0002(19)
Si(1)	0.2014(6)	¼	0.1328(2)	0.0105(9)	$Si_{1.00}$	0.011(2)	0.011(2)	0.011(2)	0.000	0.0064(17)	0.000
Si(2)	0.3556(5)	¼	0.2980(2)	0.0075(8)	$Si_{1.00}$	0.0068(19)	0.006(2)	0.011(2)	0.000	0.0047(16)	0.000
Si(3)	0.7027(6)	¾	0.1161(2)	0.0131(10)	$Si_{1.00}$	0.012(2)	0.007(2)	0.018(2)	0.000	0.0052(19)	0.000
Si(4)	0.8393(6)	¾	0.2799(2)	0.0126(9)	$Si_{1.00}$	0.011(2)	0.014(2)	0.015(2)	0.000	0.0072(18)	0.000
Si(5)	0.6719(6)	¾	0.4087(2)	0.0099(9)	$Si_{1.00}$	0.0069(19)	0.011(2)	0.009(2)	0.000	0.0015(16)	0.000
Si(6)	0.1828(6)	¼	0.4261(2)	0.0110(9)	$Si_{1.00}$	0.010(2)	0.010(2)	0.013(2)	0.000	0.0049(18)	0.000
Si(7)	0.3412(6)	¼	0.0155(2)	0.0094(9)	$Si_{1.00}$	0.012(2)	0.006(2)	0.012(2)	0.000	0.0069(17)	0.000
O(1)	0.9256(15)	¼	0.5290(5)	0.012(3)	$O_{1.00}$	0.010(5)	0.019(7)	0.008(5)	0.000	0.003(5)	0.000
H(1)	0.97(2)	¼	0.5667(10)	0.015**	$H_{1.00}$						
O(2)	0.1068(15)	¾	0.1791(5)	0.009(2)	$O_{1.00}$	0.011(5)	0.003(5)	0.012(5)	0.000	0.004(4)	0.000
H(2)	0.05(2)	¾	0.1415(12)	0.011**	$H_{1.00}$						
O(3)	0.9504(16)	¼	0.2381(5)	0.013(3)	$O_{1.00}$	0.014(6)	0.015(6)	0.007(5)	0.000	0.001(5)	0.000
H(3)	1.00(2)	¼	0.2759(8)	0.016**	$H_{1.00}$						
O(4)	0.0639(17)	¾	0.0540(6)	0.019(3)	$O_{1.00}$	0.021(7)	0.017(7)	0.021(7)	0.000	0.010(6)	0.000
O(5)	0.587(2)	¾	0.3382(7)	0.045(5)	$O_{1.00}$	0.057(12)	0.058(13)	0.010(7)	0.000	0.005(7)	0.000
O(6)	0.2384(12)	0.4930(18)	0.0127(4)	0.020(2)	$O_{1.00}$	0.021(4)	0.014(5)	0.026(5)	0.006(4)	0.011(4)	0.004(4)
O(7)	0.374(2)	¼	−0.0433(7)	0.035(4)	$O_{1.00}$	0.050(10)	0.040(11)	0.014(7)	0.000	0.012(7)	0.000
O(8)	0.4848(17)	¼	0.2712(7)	0.031(4)	$O_{1.00}$	0.011(6)	0.052(11)	0.035(8)	0.000	0.015(6)	0.000
O(9)	0.0559(16)	¼	0.4587(6)	0.015(3)**	$O_{1.00}$						
O(10)	0.9676(14)	¾	0.2487(6)	0.013(3)	$O_{1.00}$	0.005(5)	0.007(6)	0.026(7)	0.000	0.006(5)	0.000
O(11)	0.0944(15)	¼	0.1708(6)	0.012(2)	$O_{1.00}$	0.013(6)	0.009(6)	0.018(6)	0.000	0.011(5)	0.000
O(12)	0.3041(12)	0.4748(18)	0.4442(5)	0.022(2)	$O_{1.00}$	0.021(5)	0.010(5)	0.041(6)	−0.003(4)	0.021(4)	−0.004(4)
O(13)	0.8140(11)	0.5129(16)	0.1421(4)	0.0166(18)	$O_{1.00}$	0.017(4)	0.008(4)	0.019(4)	−0.005(4)	0.004(3)	0.000(4)
O(14)	0.3271(10)	0.4784(17)	0.1476(4)	0.0143(18)	$O_{1.00}$	0.012(4)	0.018(5)	0.014(4)	−0.007(4)	0.007(3)	−0.005(4)
O(15)	0.7842(10)	0.5123(16)	0.4332(4)	0.0152(18)	$O_{1.00}$	0.008(4)	0.010(4)	0.023(4)	0.001(4)	0.004(3)	0.002(3)
O(16)	0.7138(12)	0.5231(17)	0.2597(4)	0.0186(19)	$O_{1.00}$	0.026(5)	0.011(5)	0.031(5)	0.003(4)	0.023(4)	−0.002(4)
O(17)	0.0541(16)	¼	0.0621(6)	0.021(3)	$O_{1.00}$	0.010(6)	0.025(8)	0.020(7)	0.000	−0.001(5)	0.000
O(18)	0.2419(11)	0.4883(16)	0.2763(4)	0.0173(19)	$O_{1.00}$	0.013(4)	0.005(4)	0.025(5)	0.001(4)	0.001(4)	0.000(3)
O(19)	0.5174(15)	¼	0.0727(5)	0.012(2)**	$O_{1.00}$						
O(20)	0.5534(19)	¾	0.1341(7)	0.031(4)	$O_{1.00}$	0.020(7)	0.048(11)	0.033(8)	0.000	0.018(7)	0.000
O(21)	0.452(3)	¼	0.3682(7)	0.050(5)	$O_{1.00}$	0.054(12)	0.066(15)	0.012(7)	0.000	−0.001(7)	0.000
O(22)	0.536(2)	¾	0.4343(7)	0.038(4)	$O_{1.00}$	0.020(8)	0.065(14)	0.030(8)	0.000	0.013(7)	0.000
O(23)	0.060(3)	0.319(3)	0.3570(8)	0.024(5)	$O_{0.50}$	0.036(10)	0.013(10)	0.014(8)	−0.001(6)	0.003(8)	0.006(7)
O(24)	0.959(2)	0.817(3)	0.3500(8)	0.019(4)	$O_{0.50}$	0.021(8)	0.019(12)	0.021(8)	−0.002(7)	0.013(7)	−0.004(7)

*Fixed during the refinement. In radekškodaite-(La) for *M*(1) Al *vs.* Fe was refined (e_{ref} 17.50), for *M*(3) Fe *vs.* Mg was refined (e_{ref} 23.40). Thus, on the basis of chemical data and e_{ref} the *M*(1) site was assumed to be occupied by ($Al_{0.49}Fe^{3+}_{0.36}Mg_{0.15}$) possibly with a minor Ti^{4+} admixture; *M*(3) octahedron – by ($Fe^{2+}_{0.57}Mg_{0.18}Mn_{0.14}Fe^{3+}_{0.11}$); in radekškodaite-(Ce) for the *A*(1) site Ca *vs.* Ce was refined (e_{ref} 22.89), for *M*(1) Al *vs* Fe was refined (e_{ref} 15.86). Thus, on the basis of chemical data and e_{ref} the *A*(1) site was assumed to be occupied by ($Ca_{0.79}Mn_{0.16}REE_{0.05}$) and the *M*(1) site by ($Al_{0.62}Fe^{3+}_{0.23}Mg_{0.15}$) possibly with a minor Ti^{4+} admixture.
**U_{iso}.

epidote; more commonly, radekškodaite is missing in this scheme. In other words, members of the torneböhmite–epidote series alternate in the following order from the centre towards the margin of the nodule: **T → ET2 → ET → E**. The typical feature of the Mochalin Log *REE* assemblage is its enrichment in *LREE*, especially La and Ce, and very strong depletion in *HREE* and Y resulting in the situation when the contents of Y and any *REE* heavier than Sm is below its detection limit by EMPA (Kasatkin *et al.*, 2020b and references therein). Composition of *REE* in radekškodaite follows the same trend (Figs 7 and 8). Such similar distribution of *REE* in many minerals belonging to various structure types indicates that is probably caused by the general geochemistry of the mineral-forming system. The origin of this geochemical feature (which could be named a 'lanthanum anomaly') at Mochalin Log is not in the scope of the present work. However, some local differences in distribution of individual lanthanides between coexisting minerals were observed and reflect the affinities of representatives of different structure types to La^{3+} or REE^{3+} with smaller ionic radii. For example, *REE* enter mainly the *A*(2)–*A*(6) sites in radekškodaite and *A*(2)–*A*(4) in (ferri) perbøeite, and the average *REE*–O distance in radekškodaite is ~2% larger than in (ferri)perbøeite (cf. Kasatkin *et al.*, 2020b). This difference could cause preferential incorporation of La into radekškodaites as compared to (ferri)perbøeite and be responsible for the coexistence of radekškodaite-(La) with (ferri) perbøeite-(Ce).

A mineral corresponding by chemical composition to a Ce-dominant member of **ET2**-type has been found recently by R. Škoda (pers. comm.) at Nya Bastnäs deposit, Bergslagen, Sweden. It occurs as thin lammellae (up to 10 µm thick) embedded in ferriperbøeite-(Ce). Associated minerals include torneböhmite-(Ce), ferriallanite-(Ce) bastnäsite-(Ce) and cerite-(Ce).

https://doi.org/10.1180/mgm.2020.64 Published online by Cambridge University Press

Table 7. Selected interatomic distances (Å) and Si–O–Si angle (°) for radekškodaite-(La) and radekškodaite-(Ce).

Radekškodaite-(La)				Radekškodaite-(Ce)			
A(1)–O(19)	2.331(9)	*A*(4)–O(19)	2.382(8)	*A*(1)–O(13)	2.358(9)×2	*A*(4)–O(19)	2.345(12)
A(1)–O(13)	2.368(6)×2	*A*(4)–O(16)	2.455(6)×2	*A*(1)–O(19)	2.375(13)	*A*(4)–O(16)	2.439(10)×2
A(1)–O(6)	2.393(6)×2	*A*(4)–O(3)	2.672(6)×2	*A*(1)–O(6)	2.399(10)×2	*A*(4)–O(14)	2.686(13)
A(1)–O(17)	2.539(8)	*A*(4)–O(14)	2.695(8)	*A*(1)–O(17)	2.567(15)	*A*(4)–O(3)	2.693(9)×2
A(1)–O(11)	2.914(8)	*A*(4)–O(13)	2.754(6)×2	*A*(1)–O(11)	2.936(13)	*A*(4)–O(13)	2.741(10)×2
A(1)–O(7)	3.096(4)×2	*A*(4)–O(20)	2.996(3)×2	*A*(1)–O(7)	3.078(7)×2	*A*(4)–O(20)	3.007(5)×2
<*A*(1)–O>	2.611	*A*(4)–O(8)	3.034(9)	<*A*(1)–O>	2.616	*A*(4)–O(8)	3.103(15)
		<*A*(4)–O>	2.715			<*A*(4)–O>	2.718
A(2)–O(21)	2.297(9)			*A*(2)–O(21)	2.294(16)		
A(2)–O(12)	2.482(6)×2	*A*(5)–O(8)	2.432(9)	*A*(2)–O(12)	2.483(10)×2	*A*(5)–O(8)	2.417(15)
A(2)–O(1)	2.678(8)	*A*(5)–O(23)	2.526(12)	*A*(2)–O(1)	2.673(12)	*A*(5)–O(23)	2.52(2)
A(2)–O(12)	2.680(6)×2	*A*(5)–O(16)	2.552(6)×2	*A*(2)–O(12)	2.690(10)×2	*A*(5)–O(16)	2.556(9)×2
A(2)–O(15)	2.749(6)×2	*A*(5)–O(15)	2.584(6)×2	*A*(2)–O(15)	2.741(9)×2	*A*(5)–O(15)	2.586(9)×2
A(2)–O(22)	2.972(3)×2	*A*(5)–O(9)	2.824(8)	*A*(2)–O(22)	2.965(5)×2	*A*(5)–O(9)	2.815(13)
A(2)–O(22)	3.059(9)	*A*(5)–O(24)	2.972(10)	*A*(2)–O(22)	3.099(16)	*A*(5)–O(24)	2.972(19)
<*A*(2)–O>	2.709	*A*(5)–O(21)	3.074(12)	<*A*(2)–O>	2.711	*A*(5)–O(21)	3.13(2)
		A(5)–O(5)	3.276(6)×2			*A*(5)–O(5)	3.252(10)×2
A(3)–O(5)	2.296(9)	<*A*(5)–O>	2.787	*A*(3)–O(5)	2.292(15)	<*A*(5)–O>	2.786
A(3)–O(14)	2.532(5)×2			*A*(3)–O(14)	2.535(9)×2		
A(3)–O(2)	2.620(8)	*A*(6)–O(22)	2.429(9)	*A*(3)–O(2)	2.597(12)	*A*(6)–O(22)	2.423(16)
A(3)–O(16)	2.676(6)×2	*A*(6)–O(12)	2.498(6)×2	*A*(3)–O(16)	2.673(9)×2	*A*(6)–O(12)	2.504(10)×2
A(3)–O(18)	2.757(6)×2	*A*(6)–O(24)	2.549(11)	*A*(3)–O(18)	2.756(10)×2	*A*(6)–O(24)	2.511(18)
A(3)–O(8)	2.959(2)×2	*A*(6)–O(18)	2.559(6)×2	*A*(3)–O(8)	2.956(4)×2	*A*(6)–O(18)	2.560(10)×2
A(3)–O(20)	3.159(8)	*A*(6)–2.789(13)	2.779(8)	*A*(3)–O(20)	3.235(15)	*A*(6)–O(10)	2.789(13)
<*A*(3)–O>	2.720	*A*(6)–O(23)	2.970(11)	<*A*(3)–O>	2.724	*A*(6)–O(23)	2.96(2)
		A(6)–O(5)	3.274(11)			*A*(6)–O(5)	3.33(2)
M(1)–O(4)	1.879(5)×2	*A*(6)–O(21)	3.376(6)×2	*M*(1)–O(4)	1.873(9)×2	*A*(6)–O(21)	3.348(12)×2
M(1)–O(6)	2.022(6)×2	<*A*(6)–O>	2.806	*M*(1)–O(6)	2.007(10)×2	<*A*(6)–O>	2.803
M(1)–O(17)	2.025(5)×2			*M*(1)–O(17)	2.015(9)×2		
<*M*(1)–O>	1.975	*M*(3)–O(20)	1.986(10)	<*M*(1)–O>	1.965	*M*(3)–O(20)	1.942(16)
		M(3)–O(4)	2.022(9)			*M*(3)–O(4)	1.998(14)
M(2)–O(3)	1.886(6)	*M*(3)–O(14)	2.174(6)×2	*M*(2)–O(3)	1.883(9)	*M*(3)–O(14)	2.136(10)×2
M(2)–O(2)	1.892(6)	*M*(3)–O(6)	2.260(6)×2	*M*(2)–O(2)	1.883(9)	*M*(3)–O(6)	2.228(10)×2
M(2)–O(13)	1.896(6)	<*M*(3)–O>	2.146	*M*(2)–O(13)	1.893(9)	<*M*(3)–O>	2.111
M(2)–O(18)	1.915(6)			*M*(2)–O(18)	1.913(9)		
M(2)–O(11)	1.938(5)	*M*(4)–O(1)	1.877(5)×2	*M*(2)–O(11)	1.943(9)	*M*(4)–O(1)	1.857(8)×2
M(2)–O(10)	1.961(6)	*M*(4)–O(15)	1.909(6)×2	*M*(2)–O(10)	1.967(10)	*M*(4)–O(15)	1.910(8)×2
<*M*(2)–O>	1.915	*M*(4)–O(9)	1.962(6)×2	<*M*(2)–O>	1.914	*M*(4)–O(9)	1.958(9)×2
		<*M*(4)–O>	1.916			<*M*(4)–O>	1.908
Si(1)–O(14)	1.629(6)×2			Si(1)–O(11)	1.632(13)		
Si(1)–O(11)	1.644(8)	Si(5)–O(5)	1.593(9)	Si(1)–O(14)	1.652(10)×2	Si(5)–O(5)	1.585(16)
Si(1)–O(17)	1.662(8)	Si(5)–O(22)	1.601(10)	Si(1)–O(17)	1.671(14)	Si(5)–O(22)	1.613(16)
<Si(1)–O>	1.641	Si(5)–O(15)	1.643(6)×2	<Si(1)–O>	1.652	Si(5)–O(15)	1.635(9)×2
		<Si(5)–O>	1.620			<Si(5)–O>	1.617
Si(2)–O(21)	1.581(9)			Si(2)–O(21)	1.579(16)		
Si(2)–O(8)	1.611(9)	Si(6)–O(12)	1.624(6)×2	Si(2)–O(8)	1.582(15)	Si(6)–O(12)	1.609(10)×2
Si(2)–O(18)	1.641(6)×2	Si(6)–O(23)	1.632(11)	Si(2)–O(18)	1.639(9)×2	Si(6)–O(23)	1.634(18)
<Si(2)–O>	1.619	Si(6)–O(9)	1.664(8)	<Si(2)–O>	1.610	Si(6)–O(9)	1.677(14)
		Si(6)–O>	1.636	Si(3)–O(20)	1.594(15)	<Si(6)–O>	1.632
Si(3)–O(20)	1.595(9)			Si(3)–O(13)	1.632(10)×2		
Si(3)–O(13)	1.633(6)×2	Si(7)–O(19)	1.607(8)	Si(3)–O(7)	1.643(15)	Si(7)–O(19)	1.588(13)
Si(3)–O(7)	1.640(9)	Si(7)–O(7)	1.636(9)	<Si(3)–O>	1.625	Si(7)–O(7)	1.630(16)
<Si(3)–O>	1.625	Si(7)–O(6)	1.638(6)×2			Si(7)–O(6)	1.649(10)×2
		<Si(7)–O>	1.630	Si(4)–O(16)	1.638(10)×2	<Si(7)–O>	1.629
Si(4)–O(16)	1.626(6)×2			Si(4)–O(24)	1.645(18)		
Si(4)–O(24)	1.641(11)			Si(4)–O(10)	1.659(13)		
Si(4)–O(10)	1.671(8)	Si(7)–O(7)–Si(3)	148.9(6)	<Si(4)–O>	1.645	Si(7)–O(7)–Si(3)	149.0(13)
<Si(4)–O>	1.641						

Table 8. Hydrogen-bond lengths (*d* in Å) and angles (in °)

Radekškodaite-(La)					Radekškodaite-(Ce)				
D– H···*A*	*D*–H	H···*A*	*D*···*A*	∠(*D*–H···*A*)	*D*–H···*A*	*D*–H	H···*A*	*D*···*A*	∠(*D*–H···*A*)
O(1)–H(1)···O(24)	0.850(11)	1.90(4)	2.718(13)	161(13)	O(1)–H(1)···O(24)	0.849(11)	1.93(3)	2.77(2)	168(8)
O(2)–H(2)···O(4)	0.851(10)	2.13(5)	2.968(12)	169(22)	O(2)–H(2)···O(4)	0.850(10)	2.26(12)	2.994(18)	145(18)
O(3)–H(3)···O(23)	0.849(11)	1.89(4)	2.710(13)	162(11)	O(3)–H(3)···O(23)	0.850(10)	1.90(4)	2.73(2)	165(13)

D – donor; *A* – acceptor.

https://doi.org/10.1180/mgm.2020.64 Published online by Cambridge University Press

Table 9. Bond-valence calculations for radekškodaite-(La) and radekškodaite-(Ce). Parameters were taken from Gagné and Hawthorne (2015) and from Ferraris and Ivaldi (1988) for H bonding.

Radekškodaite-(La)

	A(1)	*A*(2)	*A*(3)	*A*(4)	*A*(5)	*A*(6)	*M*(1)	*M*(2)	*M*(3)	*M*(4)	Si(1)	Si(2)	Si(3)	Si(4)	Si(5)	Si(6)	Si(7)	Σ	H-bonding	Σ
O(1)		0.25								$0.55^{\times 2\downarrow\rightarrow}$								1.35	−0.23(O24)	1.12
O(2)			0.29					$0.52^{\times 2\rightarrow}$										1.33	−0.14(O4)	1.19
O(3)				0.24				$0.53^{\times 2\rightarrow}$										1.30	−0.22(O23)	1.08
O(4)							$0.60^{\times 2\downarrow\rightarrow}$		0.44									1.64	+0.14(O2)	1.78
O(5)			0.72		$0.05^{\times 2\downarrow\rightarrow}$	0.05									1.08			1.95		1.95
O(6)	$0.31^{\times 2\downarrow}$						$0.41^{\times 2\downarrow}$		$0.26^{\times 2\downarrow}$								$0.96^{\times 2\downarrow}$	1.94		1.94
O(7)	$0.05^{\times 2\downarrow\rightarrow}$												0.96				0.97	2.03		2.03
O(8)			$0.11^{\times 2\downarrow\rightarrow}$	0.09	0.49							1.03						1.83		1.83
O(9)					0.17					$0.44^{\times 2\downarrow\rightarrow}$						0.90		1.95		1.95
O(10)						0.19		$0.45^{\times 2\rightarrow}$						0.89				1.98		1.98
O(11)	0.09							$0.47^{\times 2\rightarrow}$			0.95							1.98		1.98
O(12)		$0.43^{\times 2\downarrow}$, $0.25^{\times 2\downarrow}$				$0.41^{\times 2\downarrow}$										$1.00^{\times 2\downarrow}$		2.09		2.09
O(13)	$0.34^{\times 2\downarrow}$			$0.20^{\times 2\downarrow}$				0.52					$0.98^{\times 2\downarrow}$					2.04		2.04
O(14)			$0.37^{\times 2\downarrow}$	$0.25^{\times 2\downarrow}$					$0.31^{\times 2\downarrow}$		$0.99^{\times 2\downarrow}$							1.92		1.92
O(15)		$0.20^{\times 2\downarrow}$			$0.32^{\times 2\downarrow}$					$0.51^{\times 2\downarrow}$					$0.95^{\times 2\downarrow}$			1.98		1.98
O(16)			$0.25^{\times 2\downarrow}$	$0.46^{\times 2\downarrow}$	$0.35^{\times 2\downarrow}$									$0.99^{\times 2\downarrow}$				2.05		2.05
O(17)	0.22						$0.41^{\times 2\downarrow\rightarrow}$				0.91							1.95		1.95
O(18)			$0.20^{\times 2\downarrow}$			$0.35^{\times 2\downarrow}$		0.50				$0.96^{\times 2\downarrow}$						2.01		2.01
O(19)	0.37			0.57													1.04	1.98		1.98
O(20)			0.07	$0.10^{\times 2\downarrow\rightarrow}$					0.49				1.08					1.84		1.84
O(21)		0.72			0.08	$0.04^{\times 2\downarrow\rightarrow}$						1.12						2.00		2.00
O(22)		$0.11^{\times 2\downarrow\rightarrow}$, 0.09				0.50									1.06			1.78		1.78
O(23)					0.42	$0.04^{\times 2\downarrow\rightarrow}$										1.12		1.62	+0.24(O3)	1.86
O(24)					$0.04^{\times 2\downarrow\rightarrow}$	0.38								1.06				1.52	+0.23(O1)	1.75
Σ	2.08	3.04	2.94	2.92	2.67	2.81	2.84	2.99	2.07	3.00	3.84	4.07	4.00	3.83	4.04	3.88	3.93			

The values were calculated taking into account the refined occupancies for the *M*(1–4) and *A*(1) sites. For Fe cations in the *M*(3) site the bond-valence parameters of Fe^{2+} was used. The bond-valence parameters of La^{3+} were used for *A*(1–6) sites for radekškodaite-(La) and Ce^{3+} for radekškodaite-(Ce). For better clarity the split character of the O(23) and O(24) sites was not taken into account and these sites were considered as averaged with no splitting (the cations–O(23)/O(24) distances for bond-valence calculations including H bonding were taken for non-split sites).

Table 9. (*Continued.*)

Radekškodaite-(Ce)

	A(1)	*A*(2)	*A*(3)	*A*(4)	*A*(5)	*A*(6)	*M*(1)	*M*(2)	*M*(3)	*M*(4)	Si(1)	Si(2)	Si(3)	Si(4)	Si(5)	Si(6)	Si(7)	Σ	H-bonding	Σ
O(1)		0.24								$0.57^{\times 2\downarrow\rightarrow}$								1.38	−0.21(O24)	1.17
O(2)			0.29					$0.54^{\times 2\rightarrow}$										1.37	−0.13(O4)	1.24
O(3)				0.23				$0.54^{\times 2\rightarrow}$										1.31	−0.24(O23)	1.07
O(4)							$0.59^{\times 2\downarrow\rightarrow}$		0.45									1.63	+0.13(O2)	1.76
O(5)			0.63		$0.05^{\times 2\downarrow\rightarrow}$	0.04									1.11			1.88		1.88
O(6)	$0.29^{\times 2\downarrow}$						$0.42^{\times 2\downarrow}$		$0.27^{\times 2\downarrow}$								$0.94^{\times 2\downarrow}$	1.92		1.92
O(7)	$0.06^{\times 2\downarrow\rightarrow}$												0.95				0.98	2.05		2.05
O(8)			$0.11^{\times 2\downarrow\rightarrow}$	0.08	0.46							1.11						1.87		1.87
O(9)					0.16					$0.45^{\times 2\downarrow\rightarrow}$						0.87		1.93		1.93
O(10)						0.18		$0.43^{\times 2\rightarrow}$						0.91				1.95		1.95
O(11)	0.08							$0.46^{\times 2\rightarrow}$			0.98							1.98		1.98
O(12)		$0.39^{\times 2\downarrow}$, $0.23^{\times 2\downarrow}$				$0.37^{\times 2\downarrow}$										$1.04^{\times 2\downarrow}$		2.03		2.03
O(13)	$0.33^{\times 2\downarrow}$			$0.20^{\times 2\downarrow}$				0.53					$0.98^{\times 2\downarrow}$					2.04		2.04
O(14)			$0.34^{\times 2\downarrow}$	$0.23^{\times 2\downarrow}$					$0.33^{\times 2\downarrow}$		$0.93^{\times 2\downarrow}$							1.83		1.83
O(15)		$0.20^{\times 2\downarrow}$			$0.30^{\times 2\downarrow}$					$0.51^{\times 2\downarrow}$					$0.97^{\times 2\downarrow}$			1.98		1.98
O(16)			$0.24^{\times 2\downarrow}$	$0.43^{\times 2\downarrow}$	$0.32^{\times 2\downarrow}$									$0.98^{\times 2\downarrow}$				1.97		1.97
O(17)	0.20						$0.41^{\times 2\downarrow\rightarrow}$				0.89							1.91		1.91
O(18)			$0.19^{\times 2\downarrow}$			$0.32^{\times 2\downarrow}$		0.49				$0.96^{\times 2\downarrow}$						1.96		1.96
O(19)	0.31			0.55													1.10	1.96		1.96
O(20)			0.06	$0.10^{\times 2\downarrow\rightarrow}$					0.52				1.08					1.86		1.86
O(21)		0.63			0.07	$0.04^{\times 2\downarrow\rightarrow}$						1.12						1.90		1.90
O(22)		$0.11^{\times 2\downarrow\rightarrow}$, 0.08				0.45									1.03			1.78		1.78
O(23)					0.38	$0.05^{\times 2\downarrow\rightarrow}$										1.11		1.59	+0.23(O3)	1.82
O(24)					$0.05^{\times 2\downarrow\rightarrow}$	0.39								1.06				1.55	+0.21(O1)	1.76
Σ	1.95	2.81	2.74	2.78	2.51	2.62	2.84	2.99	2.17	3.06	3.73	4.15	3.99	3.93	4.08	4.06	3.96			

The values were calculated taking into account the refined occupancies for the *M*(1–4) and *A*(1) sites. For Fe cations in the *M*(3) site the bond-valence parameters of Fe^{2+} was used. The bond-valence parameters of La^{3+} were used for *A*(1–6) sites for radekškodaite-(La) and Ce^{3+} for radekškodaite-(Ce). For better clarity the split character of the O(23) and O(24) sites was not taken into account and these sites were considered as averaged with no splitting (the cations–O(23)/O(24) distances for bond-valence calculations including H bonding were taken for non-split sites).

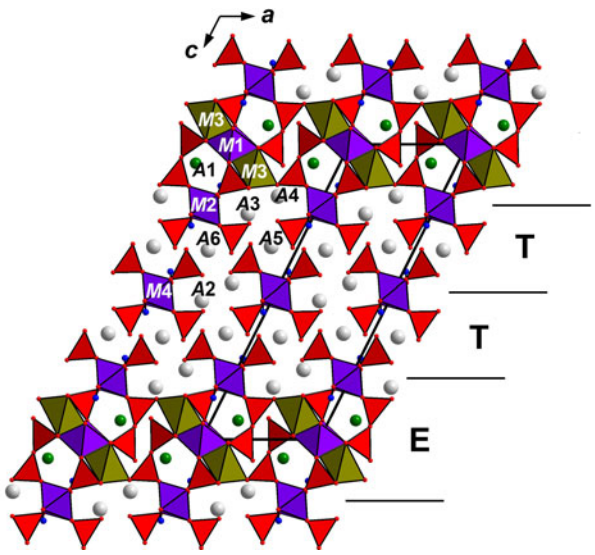

Fig. 6. The crystal structure of both radekškodaite-(La) and radekškodaite-(Ce). SiO_4 tetrahedra are red. H atoms of OH groups are shown as small blue circles. Alternation of epidote-type slabs (**E**) and törnebohmite-type slabs (**T**) is shown. The unit cell is outlined.

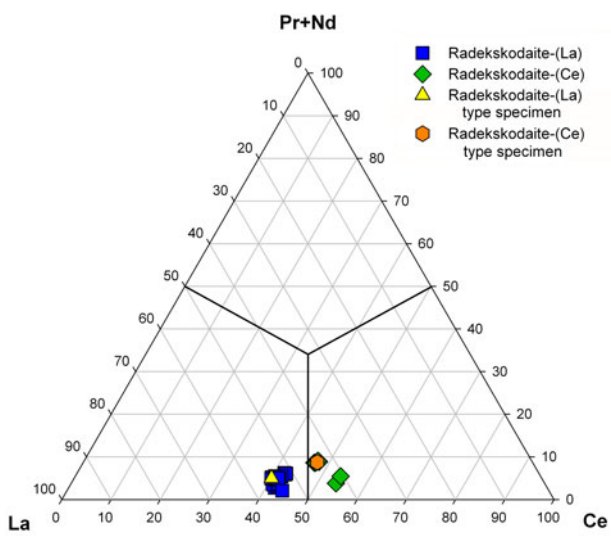

Fig. 7. Ternary plot showing distribution of *REE* at *A* sites in radekškodaite-(La) and radekškodaite-(Ce).

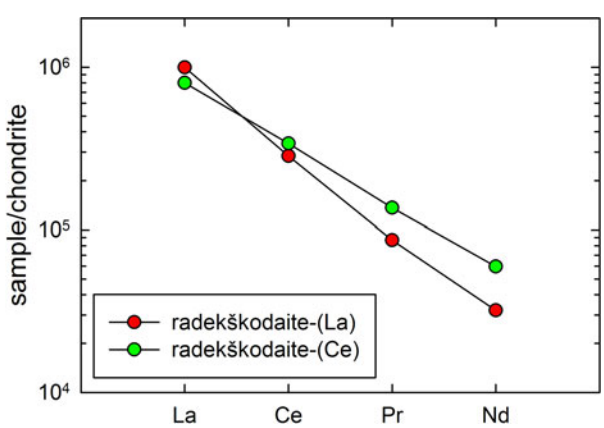

Fig. 8. Distribution of *REE* (chondrite-normalised; McDonough and Sun, 1995) in radekškodaite-(La) and radekškodaite-(Ce).

The average composition of this mineral is (electron microprobe, wt.%; Fe^{2+}/Fe^{3+} ratio calculated from charge balance, H_2O – by stochiometry): CaO 3.30, La_2O_3 17.42, Ce_2O_3 26.37, Pr_2O_3 2.07, Nd_2O_3 5.46, MgO 1.97, MnO 0.09, FeO 1.10, Al_2O_3 8.79, Fe_2O_3 5.79, SiO_2 26.09, F 0.16, H_2O 1.60, –O=F –0.07, total 100.14. The empirical formula calculated on the basis of 18 cations and $O_{28}(OH,F)_3$ is: $(Ca_{0.95}Ce_{2.59}La_{1.72}Nd_{0.52}Pr_{0.20}Mn_{0.02})_{\Sigma 6.00}(Al_{2.78}Fe^{3+}_{1.17}Mg_{0.79}Fe^{2+}_{0.25})_{\Sigma 4.99}Si_7O_{28}(OH_{2.86}F_{0.14})$ (data kindly provided by R. Škoda). The tiny size of grains precludes the structural investigation of this mineral, however, its structural relation with radekškodaite is very likely.

Supplementary material. To view supplementary material for this article, please visit: https://doi.org/10.1180/mgm.2020.64.

Acknowledgements. Dr Radek Škoda is acknowledged for his valuable help in collecting WDS and Raman data of the new minerals, and for discussion and useful advice. We thank Associate Editor Irina Galuskina, Structure Editor Daniel Atencio, Principal Editor Stuart Mills and two anonymous referees for constructive comments that improved the quality of the manuscript. This study was supported by the Russian Foundation for Basic Research, grant no. 18-05-00332 (in part of XRD structure studies and crystal chemistry). This work was partly performed in accordance with the state task, state registration no. AAA-A19-119092390076-7 for N.V.C. The technical support by the SPbSU X-Ray Diffraction Resource Center in the powder XRD study is acknowledged.

References

Agilent Technologies (2014) *CrysAlisPro Software system, version 1.171.37.34.* Agilent Technologies UK Ltd, Oxford, UK.

Allaz J., Raschke M.B., Persson P.M. and Stern C.R. (2015) Age, petrochemistry, and origin of a REE-rich mineralization in the Longs Peak-St. Vrain batholith, near Jamestown, Colorado (USA). *American Mineralogist*, **100**, 2123–2140.

Andersson U.B. (2004) The Bastnäs-type *REE*-mineralisations in northwestern Bergslagen, Sweden. *Sveriges Geologiska Undersökning Rapporter and Meddelanden*, **119**, 34.

Andò S. and Garzanti E. (2014) Raman spectroscopy in heavy-mineral studies. *Geological Society of London, Special Publications*, **386**, 395–412.

Bindi L., Holstam D., Fantappiè G., Andersson U.B. and Bonazzi P. (2018) Ferriperbøeite-(Ce), $[CaCe_3]_{\Sigma=4}[Fe^{3+}Al_2Fe^{2+}]_{\Sigma=4}[Si_2O_7][SiO_4]_3O(OH)_2$, a new member of the polysomatic epidote–törnebohmite series from the Nya Bastnäs Fe–Cu–REE deposit, Sweden. *European Journal of Mineralogy*, **30**, 537–544.

Bonazzi P., Bindi L. and Parodi G. (2003) Gatelite-(Ce), a new *REE*-bearing mineral from Trimouns, French Pyrenees: crystal structure and polysomatic relationships with epidote and törnebohmite-(Ce). *American Mineralogist*, **88**, 223–228.

Bonazzi P., Lepore G.O., Bindi L., Chopin C., Husdal T. and Medenbach O. (2014) Perbøeite-(Ce) and alnaperbøeite-(Ce), two new members of the epidote–törnebohmite polysomatic series: Chemistry, structure, dehydrogenation, and clue for a sodian epidote end-member. *American Mineralogist*, **99**, 157–169.

Bonazzi P., Holstam D. and Bindi L. (2019) Gatelite-supergroup minerals: recommended nomenclature and review. *European Journal of Mineralogy*, **31**, 173–181.

Breiter K., Čopjaková R. and Škoda R. (2009) The involvement of F, CO_2, and As in the alteration of Zr–Th–*REE*-bearing accessory minerals in the Hora Svaté Kateřiny A-type granite, Czech Republic. *The Canadian Mineralogist*, **47**, 1375–1398.

Britvin S.N., Dolivo-Dobrovolsky D.V. and Krzhizhanovskaya M.G. (2017) Software for processing the X-ray powder diffraction data obtained from the curved image plate detector of Rigaku RAXIS Rapid II diffractometer. *Zapiski Rossiiskogo Mineralogicheskogo Obshchestva*, **146**, 104–107 [in Russian].

Čopjaková R., Škoda R., Vašinová Galiová M. and Novák M. (2013) Distributions of Y plus *REE* and Sc in tourmaline and their implications for the melt

evolution; examples from NYF pegmatites of the Třebíč Pluton, Moldanubian Zone, Czech Republic. *Journal of Geosciences*, **58**, 113–131.

Čopjaková R., Škoda R., Vašinová Galiová M., Novák M. and Cempírek J. (2015) Sc- and *REE*-rich tourmaline replaced by Sc-rich *REE*-bearing epidote-group mineral from the mixed (NYF plus LCT) Kracovice pegmatite (Moldanubian Zone, Czech Republic). *American Mineralogist*, **100**, 1434–1451.

Ferraris G. and Ivaldi G. (1988) Bond valence *vs*. bond length in O…O hydrogen bonds. *Acta Crystallographica*, **B44**, 341–344.

Finger F., Broska I., Roberts M. P., Schermaier A. (1998) Replacement of primary monazite by apatite-allanite-epidote coronas in an amphibolite facies granite gneiss from the eastern Alps. *American Mineralogist*, **83**, 248–258.

Gagné O.C. and Hawthorne F.C. (2015) Comprehensive derivation of bond-valence parameters for ion pairs involving oxygen. *Acta Crystallographica*, **B71**, 562–578.

Holtstam D., Kolitsch U. and Andersson U.B. (2005) Västmanlandite-(Ce) – a new lanthanide- and F-bearing sorosilicate mineral from Västmanland, Sweden: description, crystal structure, and relation to gatelite-(Ce). *European Journal of Mineralogy*, **17**, 129–141.

Hönig S., Čopjaková R., Škoda R., Novák M., Dolejš D., Leichmann J. and Vašinová Galiová M. (2014) Garnet as a major carrier of the Y and *REE* in the granitic rocks: An example from the layered anorogenic granite in the Brno Batholith, Czech Republic. *American Mineralogist*, **99**, 1922–1941.

Kasatkin A.V., Pekov I.V., Zubkova N.V., Chukanov N.V., Polekhovsky Y.S., Belakovskiy D.I., Ksenofontov D.A., Agakhanov A.A., Kuznetsov A.M. and Pushcharovsky D.Y. (2018) Radekškodaite-(La), IMA 2018-107. *CNMNC Newsletter No. 46, December 2018, page 1377; Mineralogical Magazine*, **82**, 1369–1379.

Kasatkin A.V., Zubkova N.V., Pekov I.V., Chukanov N.V., Škoda R., Agakhanov A.A., Belakovskiy D.I. and Pushcharovsky D.Y. (2019a) Alexkuznetsovite-(La), IMA 2019–081. CNMNC Newsletter No.52. *Mineralogical Magazine*, **83**, 887–893.

Kasatkin, A.V., Zubkova, N.V., Pekov, I.V., Chukanov, N.V., Škoda, R., Nestola, F., Agakhanov, A.A., Belakovskiy, D.I. and Kuznetsov, A.M. (2019b) Radekškodaite-(Ce), IMA 2019-042. CNMNC Newsletter No. 51; CNMNC Newsletter No. 51; *Mineralogical Magazine*, **83**, 757–761

Kasatkin A.V., Zubkova N.V., Pekov I.V., Chukanov N.V., Škoda R., Agakhanov A.A., Belakovskiy D.I. and Pushcharovsky D.Y. (2020a) Alexkuznetsovite-(Ce), IMA 2019–118. CNMNC Newsletter No. 54. *Mineralogical Magazine*, **84**, 359–365.

Kasatkin A.V., Zubkova N.V., Pekov I.V., Chukanov N.V., Škoda R., Polekhovsky Y.S., Agakhanov A.A., Belakovskiy D.I., Kuznetsov A.M., Britvin S.N. and Pushcharovsky D. Yu. (2020b) The mineralogy of the historical Mochalin Log *REE* deposit, South Urals, Russia. Part I. New gatelite-group minerals ferriperbøeite-(La), $(CaLa_3)(Fe^{3+}Al_2Fe^{2+})[Si_2O_7][SiO_4]_3O(OH)_2$, and perbøeite-(La), $(CaLa_3)(Al_3Fe^{2+})[Si_2O_7][SiO_4]_3O(OH)_2$. *Mineralogical Magazine*, **84**, 593–607.

Mandarino J.A. (1981) The Gladstone-Dale relationship. IV. The compatibility concept and its 209 application. *The Canadian Mineralogist*, **41**, 989–1002.

McDonough W.F. and Sun S. (1995) The composition of the Earth. *Chemical Geology*, **120**, 223–253.

Plášil J. and Škoda R. (2017) Crystal structure of the (*REE*)–uranyl carbonate mineral shabaite-(Nd). *Journal of Geosciences*, **62**, 97–105.

Plášil J., Petříček V., Locock A.J., Škoda R. and Burns P.C. (2018) The (3 + 3) commensurately modulated structure of the uranyl silicate mineral swamboite-(Nd), $Nd_{0.333}[(UO_2)(SiO_3OH)](H_2O)_{2.41}$. *Zeitschrift für Kristallographie-Crystalline Materials*, **233**, 223–231.

Sheldrick G.M. (2008) A short history of *SHELX*. *Acta Crystallographica*, **A64**, 112–122.

Sheldrick G.M. (2015) Crystal structure refinement with SHELXL. *Acta Crystallographica*, **C71**, 3–8.

Shen J. and Moore P.B. (1982) Törnebohmite, $RE_2Al(OH)[SiO_4]_2$: crystal structure and genealogy of RE(III)Si(IV) ↔ Ca(II)P(V) isomorphism. *American Mineralogist*, **67**, 1021–1028.

Škoda R. and Novák M. (2007) Y,*REE*,Nb,Ta,Ti-oxide (AB_2O_6) minerals from *REL-REE* euxenite-subtype pegmatites of the Třebíč Pluton, Czech Republic; substitutions and fractionation trends. *Lithos*, **95**, 43–57.

Škoda R., Novák M. and Cícha J. (2011) Uranium-niobium-rich alteration products after "pisekite", an intimate mixture of Y, *REE*, Nb, Ta, Ti-oxide minerals from the Obrazek I pegmatite, Pisek, Czech Republic. *Journal of Geosciences*, **56**, 317–325.

Škoda R., Cempírek J., Filip J., Novák M., Veselovský F. and Čtvrtlík R. (2012) Allanite-(Nd), $CaNdAl_2Fe^{2+}(SiO_4)(Si_2O_7)O(OH)$, a new mineral from Åskagen, Sweden. *American Mineralogist*, **97**, 983–988.

Škoda R., Plášil J., Jonsson E., Čopjaková R., Langhof J. and Galiová Vašinová M. (2015) Redefinition of thalénite-(Y) and discreditation of fluorthalénite-(Y): A re-investigation of type material from the Österby pegmatite, Dalarna, Sweden, and from additional localities. *Mineralogical Magazine*, **79**, 965–983.

Škoda R., Plášil J., Čopjaková R., Novák M., Jonsson E., Galiová Vašinová M. and Holtstam D. (2018) Gadolinite-(Nd), a new member of the gadolinite supergroup from Fe-*REE* deposits of Bastnäs-type, Sweden. *Mineralogical Magazine*, **82**, 133–145.